Direction finding and antenna calibration through analytical inversion of radio measurements performed using a system of two or three electric dipole antennas on a three-axis stabilized spacecraft

Baptiste Cecconi, Philippe Zarka

Direction finding and antenna calibration through analytical inversion of radio measurements performed using a system of two or three electric dipole antennas on a three-axis stabilized spacecraft

B. Cecconi and P. Zarka

Laboratoire d'Etude Spatiales et d'Instrumentation en Astrophysique, Observatoire de Paris, Meudon, France

Received 30 March 2004; revised 29 December 2004; accepted 26 January 2005; published 7 May 2005.

[1] We present an analytical inversion method to achieve direction-finding (DF) (i.e., retrieve the direction of arrival of an incoming electromagnetic wave, its flux, and its full polarization state) using radio measurements performed using a system of two or three electric dipole antennas on a three-axis stabilized spacecraft. The Radio and Plasma Wave Science (RPWS) radio receiver on board Cassini includes such instantaneous DF capabilities, and so does the Solar Terrestrial Relations Observatory (STEREO) Waves radio receiver. We also present an analytical solution of the inverse problem which consists of calibrating the electric dipole orientations and effective lengths using a known radio source. Error sources (imperfect knowledge of antenna parameters, digitization errors, signal to noise ratio, etc.) and their propagation through the analytical inversion have been studied. The typical expected accuracy of our DF inversion is 1 dB [V^2/Hz] for flux measurements, about $1-2^\circ$ for source position and a few percent for degrees of polarization. For the antenna calibration procedure the expected accuracy is of the order of 2° on antenna direction and of 1% on antenna length. We define the data selection criteria to be used during both DF analysis and antenna calibration. We also discuss the limitations of the methods and the ways to improve their accuracy.

Citation: Cecconi, B., and P. Zarka (2005), Direction finding and antenna calibration through analytical inversion of radio measurements performed using a system of two or three electric dipole antennas on a three-axis stabilized spacecraft, *Radio Sci.*, *40*, RS3003, doi:10.1029/2004RS003070.

1. Introduction

[2] The angular resolution of a telescope or radio telescope of typical size D is λ/D, with λ the wavelength of the observed wave. In the low-frequency radio range ($f \leq 10$ MHz) the Earth's ionosphere reflects out incoming cosmic radio waves, thus spacecraft measurements are necessary. Constraints of size and mass on embarked antennas impose to use antennas (monopoles or dipoles) at low frequencies, of characteristic length $L \sim 10-50$ m. The corresponding resolution is very poor, as $\lambda/L \sim 1$. There is no instantaneous angular resolution with such antennas. A more adapted description of the antenna directivity is its beaming pattern which gives the antenna gain for each direction of the space. The beaming pattern of a short dipole (the short dipole approximation requires $L \ll \lambda$) varies as $\sin^2\theta$ where θ is the angular distance between the source direction and the dipole direction. By integration of the beaming pattern over the whole space, we get the beaming solid angle, which is $8\pi/3$ *sr* for the short dipole. This solid angle represents 2/3 of the whole space directions. Thus specific techniques have been derived to retrieve angular resolution from measurements performed simultaneously over several (2 or 3) dipoles: these are named direction-finding (DF) techniques. The determination of the $\vec{k}$ vector (direction of arrival of the wave) is coupled to the determination of the wave polarization (e.g., two waves with opposed circular polarization and coming from opposite directions give the same signature). Similarly, the wave intensity and the effective dipole lengths are related. DF techniques include (1) analysis of the modulations of the signal received by one or two antennas on a spinning spacecraft

0048-6604/05/2004RS003070

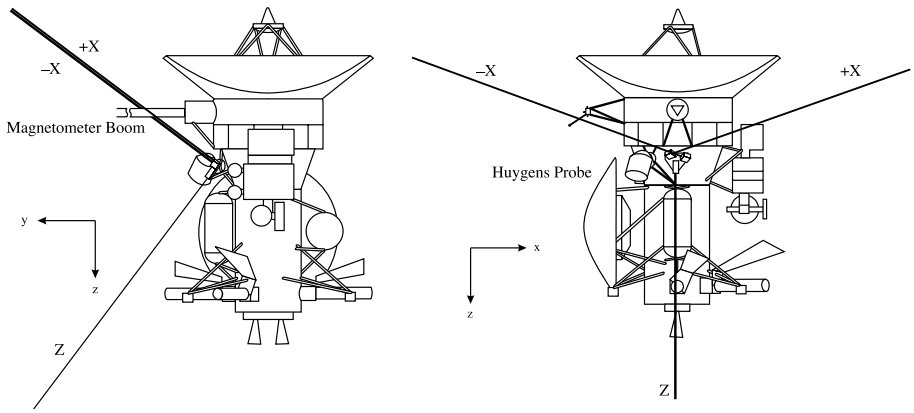

Figure 1. The Cassini spacecraft and the RPWS electrical antenna system. The three electrical antennas ($+X$, $-X$, and Z) are named according to the spacecraft reference frame. Each monopole antenna is 10 m long. The Z antenna is in the ($\vec{y}$, $\vec{z}$) plane at 37° from the $\vec{z}$ axis. The $+X$ and $-X$ antennas are separated by 120°. The ($+X$, $-X$) antenna plane makes a 70° angle with the Z antenna. In the Dipole mode the $+X$ and $-X$ antennas are coupled together in a dipole D. Figure adapted from *Vogl et al.* [2004].

[*Lecacheux*, 1978; *Ladreiter et al.*, 1994]; and (2) correlations of the signals received by two or three antennas on a three-axis stabilized spacecraft [*Lecacheux*, 1978; *Ladreiter et al.*, 1995; *Vogl et al.*, 2004].

[3] The Cassini mission is dedicated to study the environment of Saturn. One of the instruments on the orbiter is the Radio and Plasma Wave Science (RPWS) [see *Gurnett et al.*, 2004] experiment. Its high-frequency receiver (HFR) covers the 3.5 kHz to 16.1 MHz frequency range. It is composed of a set of three monopole antennas ($+X$, $-X$ and Z, see Figure 1, also referred as u, v and w antennas as in the work of *Gurnett et al.* [2004] connected to a radio receiver. The receiver measures spectral and cross-spectral powers through programmable time-frequency windows on one or two antennas. The receiver can use either the ($+X$, Z) pair of antennas, the ($-X$, Z) one or a third configuration where $+X$ and $-X$ monopoles are connected together and used as a dipole D, forming a pair (D, Z) with the monopole Z. The instantaneous data set (called hereafter two-antenna data set) consists of four measurements. For the ($+X$, Z) antenna pair, these four measurements are: two autocorrelations (1 on the Z antenna, named A_{ZZ}, and 1 on the $+X$ antenna, named A_{+XX}), and the cross correlation between the two antennas which is a complex number and provides thus two measurements: real and imaginary parts named C^r_{+XZ} and C^i_{+XZ}. For the ($-X$, Z) or (D, Z) antenna pairs, $+X$ indices must be replaced by $-X$ or D, respectively. Switching can be programmed between the two antenna configurations ($-X$, Z) and ($+X$, Z) at every other measurements at every frequency step. Such switching which simulates a three-antennas DF mode, will be primarily considered here. It provides data sets of eight measurements (consisting of two consecutive two-antenna data sets with antenna switching between ($-X$, Z) and ($+X$, Z)). The eight measurements are four autocorrelations (A_{+XX}, A_{-XX} and A_{ZZ} measured twice, one for each two-antenna data set) and two cross correlations (C^r_{+XZ}, C^i_{+XZ}, C^r_{-XZ}, C^i_{-XZ}). As A_{ZZ} is measured twice, we end up with seven independent measurements for each three-antenna data set.

[4] The purpose of a DF capable receiver is to be able to observe a radio source remotely retrieving its position, flux and polarization state. We thus concentrate on electromagnetic radio wave such as the free space propagating modes. Although electrostatic waves are also detected by the receiver, they do not propagate freely in space, so that they cannot be detected remotely. These measurements require specific treatments that are beyond the scope of the DF analysis methods we have developed. Expressing analytically the measured correlations in terms of electromagnetic wave parameters and of the antenna parameters requires the antennas to be represented as short electrical dipoles. At low frequencies (i.e., when the wavelength is very large with respect to the antenna length) we can in principle find short effective electrical dipoles equivalent to the physical monopoles. Finding these equivalent dipoles is the antenna calibration process. Each electrical antenna (n) is then fully described through three parameters: length (h_n), colatitude (θ_n) and azimuth (ϕ_n) in a reference frame (e.g., the spacecraft frame). The wave parameters are the Stokes parameter set [*Kraus*, 1966] which gives a full description of the intensity (S), the degree of linear polarization (U, Q) and degree of circular polarization (V) of the wave, and the wave vector $\vec{k}$ or direction of the

source given by its colatitude (θ) and azimuth (ϕ) in the spacecraft system frame. Thus the three antennas are described by 9 parameters and the wave by six parameters. This gives us 15 parameters in terms of which the measurements are expressed. As seen above, the three-antenna data sets used for the DF contain seven independent measurements. We thus have to make assumptions on some parameters to retrieve the others. From now on, the parameters on which assumptions will be made are called "preset parameters," the rest of them are the "unknowns." In the DF mode, the preset parameters are the antenna parameters and the unknowns are the wave parameters as discussed in section 2.1. In the calibration mode, we assume that we know some of the wave parameters and some of the antenna parameters, as discussed in section 2.2. Error sources and their propagation throughout the DF equations are studied in section 3. Data selection criteria that have to be applied to achieve the expected accuracy for both DF analysis and antenna calibration are then discussed in section 4, as well as ways to improve the accuracy of the DF and possible extensions of the method.

2. DF Analytical Inversion

[5] Considering RPWS antennas as short electrical dipoles, the output voltage at the nth antenna can be written $V_n = (\vec{h}_n.\vec{E})$, where $\vec{h}_n$ is the effective electrical antenna vector and $\vec{E}$ the electric field of the incoming wave. The receiver measures quantities such as $\langle V_n V_k^* \rangle$. These are time-averaged correlations between the voltages on the h_n and h_k antennas. The seven measurements used in the DF mode are the autocorrelations on the three antennas ($A_{+XX} = \langle V_{+X} V_{+X}^* \rangle$, $A_{-XX} = \langle V_{-X} V_{-X}^* \rangle$ and $A_{ZZ} = \langle V_Z V_Z^* \rangle$) and the cross correlations between the ($+X$, Z) pair of antenna and the ($-X$, Z) one; the last two quantities are complex numbers corresponding to four real measurements: $C^r_{+XZ} = \mathcal{R}e(\langle V_{+X} V_Z^* \rangle)$, $C^i_{+XZ} = \mathcal{I}m(\langle V_{+X} V_Z^* \rangle)$, $C^r_{-XZ} = \mathcal{R}e(\langle V_{-X} V_Z^* \rangle)$ and $C^i_{-XZ} = \mathcal{I}m(\langle V_{-X} V_Z^* \rangle)$.

[6] As done in the work of *Ladreiter et al.* [1995], the modeled measurements can be written in the following way:

$$A_{+XX} = \frac{Sh_{+X}^2}{2}\left[(1+Q)\Omega_{+X}^2 + 2U\Omega_{+X}\Psi_{+X} + (1-Q)\Psi_{+X}^2\right] \quad (1)$$

$$A_{-XX} = \frac{Sh_{-X}^2}{2}\left[(1+Q)\Omega_{-X}^2 + 2U\Omega_{-X}\Psi_{-X} + (1-Q)\Psi_{-X}^2\right] \quad (2)$$

$$A_{ZZ} = \frac{Sh_Z^2}{2}\left[(1+Q)\Omega_Z^2 + 2U\Omega_Z\Psi_Z + (1-Q)\Psi_Z^2\right] \quad (3)$$

$$C^r_{+XZ} = \frac{Sh_{+X}h_Z}{2}\left[(1+Q)\Omega_{+X}\Omega_Z + U(\Omega_{+X}\Psi_Z + \Omega_Z\Psi_{+X}) + (1-Q)\Psi_{+X}\Psi_Z\right] \quad (4)$$

$$C^i_{+XZ} = \frac{Sh_{+X}h_Z}{2}V\left[-\Omega_{+X}\Psi_Z + \Omega_Z\Psi_{+X}\right] \quad (5)$$

$$C^r_{-XZ} = \frac{Sh_{-X}h_Z}{2}\left[(1+Q)\Omega_{-X}\Omega_Z + U(\Omega_{-X}\Psi_Z + \Omega_Z\Psi_{-X}) + (1-Q)\Psi_{-X}\Psi_Z\right] \quad (6)$$

$$C^i_{-XZ} = \frac{Sh_{-X}h_Z}{2}V\left[-\Omega_{-X}\Psi_Z + \Omega_Z\Psi_{-X}\right] \quad (7)$$

where $\Omega_n = (\vec{h}_n.\vec{X}_w)/h_n$ and $\Psi_n = (\vec{h}_n.\vec{Y}_w)/h_n$ are the coordinates of the nth antenna unit vector projected on the wave plane (O, $\vec{X}_w$, $\vec{Y}_w$) (see Figure 2 for the definition of $\vec{X}_w$, $\vec{Y}_w$ and $\vec{Z}_w$), (S, Q, U, V) are the wave Stokes parameters. Ω_n and Ψ_n can be expressed in terms of the antenna parameters and of the source direction:

$$\Omega_n = \cos\theta_n \sin\theta - \sin\theta_n \cos\theta \cos(\phi - \phi_n) \quad (8)$$

$$\Psi_n = -\sin\theta_n \sin(\phi - \phi_n) \quad (9)$$

where θ_n and ϕ_n are the colatitude and azimuth of the nth antenna, and θ and ϕ the colatitude and azimuth of the source direction. Those expressions have actually been defined in the spacecraft frame [see *Ladreiter et al.*, 1995] as follows: Z_w is pointing from the source to the spacecraft, X_w is in the (z_{SC}, Z_w) plane and perpendicular to Z_w and Y_w completes the right hand orthogonal triad. Ω_n and Ψ_n are also valid in the wave frame (defined in Figure 2), taking $\theta = \pi$ and $\phi = 0$ (by definition of the frame). The antenna direction parameters (θ_n and ϕ_n) are the one of the antenna in the specified frame. These expressions thus are valid in both of these coordinate systems.

[7] As the X_w and Y_w are defining the linear polarization axes, the U and Q Stokes parameters values will actually depends on the frame (and its orientation) in which they are computed. For instance, it will depend on the spacecraft attitude when the polarization axes are defined with respect to the spacecraft axes (as with the *Ladreiter et al.* [1995] axes definition). Note that the total linear polarization degree, defined as $\sqrt{U^2+Q^2}$, remains constant anyway.

[8] The Stokes polarization parameters can be related to parameters such as the degree of polarization, sense of

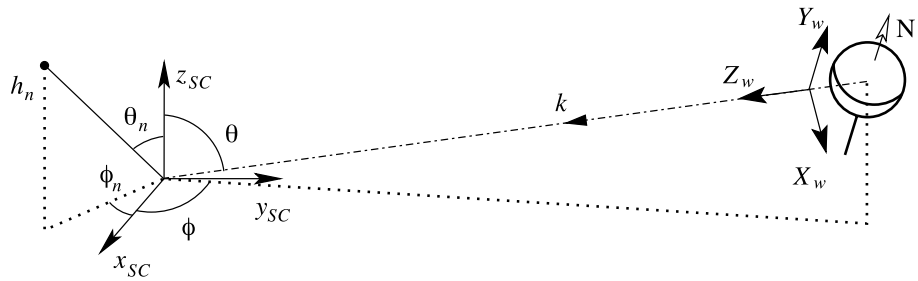

Figure 2. The wave frame ($\vec{X}_w$, $\vec{Y}_w$, $\vec{Z}_w$). Here $\vec{Z}_w$ is colinear to the wave vector $\vec{k}$; and $\vec{Y}_w$ is in the plane containing $\vec{Z}_w$ and a relevant axis of the object studied (e.g., Jupiter's rotational or magnetic axis). The source is in the (θ, ϕ) direction. Here ($\vec{x}_{SC}$, $\vec{y}_{SC}$, $\vec{z}_{SC}$) is the spacecraft reference frame. One antenna $\vec{h}_n$ is shown with its colatitude θ_n and azimuth ϕ_n.

circular polarization and orientation of the plane of linear polarization [see *Kraus*, 1966; *Hamaker and Bregman*, 1996]).

2.1. Direction Finding Analysis

[9] Assuming that the nine antenna parameters are known, a three-antenna data set contains enough information to carry out the DF analysis. Inversion methods based on least square model fitting have been developed by *Ladreiter et al.* [1995] and *Vogl et al.* [2004]. Equations (1) to (7) are not linear with respect to the unknowns. The χ^2 defined as the weighted sum of the squared differences from model to measurements will thus not be linear too and neither its first derivative. The principle of a χ^2 minimization is to follow the steepest gradients normal to the χ^2 hypersurface to converge from the initial conditions towards the χ^2 minimum. Ladreiter proposed to differentiate the first derivative of the χ^2 to get a linear relationship which can be inverted with a singular-value decomposition (SVD) method, in order to compute the steepest gradient directions at each step. Vogl used a Powell algorithm to obtain the same result, adding the ability to use several three-antenna data sets together. We present here a fully analytical inversion. This method has advantages and drawbacks that will be discussed in section 3.1. Two inversions are presented for three-antenna data sets. One works in the general case when $V \neq 0$, except for some very particular geometrical configurations. The other one deals with purely circularly polarized waves (i.e., $Q = 0$ and $U = 0$), including the unpolarized wave case (i.e., $V = 0$, $Q = 0$ and $U = 0$). We could not find an analytical inversion that works in the case of a purely linearly polarized wave (i.e., $V = 0$, $Q \neq 0$ and/or $U \neq 0$). Additionally, we discuss partial DF inversions on two-antenna data sets (assuming some wave parameters to be known).

2.1.1. General Case

[10] The system of seven equations (1)–(7) can be simplified by using an appropriate coordinate frame. We define here an ''antenna frame'' which is defined as follows: the $\vec{z}$ unit vector axis is chosen along the Z antenna and the $+X$ and $-X$ antennas have supplementary azimuths ($\phi_{-X} = \pi - \phi_{+X}$). The ($\vec{y}$, $\vec{z}$) plane is bisecting the ($\vec{h}_{+X}$, $\vec{h}_Z$) and ($\vec{h}_{-X}$, $\vec{h}_Z$) planes as shown on Figure 3. We can always build such a reference frame whatever the actual geometry of the physical monopoles. Notice that the colatitudes of the $+X$ and $-X$ antennas need not to be the same, as it is in general the case. In such a coordinate system, the cartesian coordinates of the three antennas are:

$$\vec{h}_Z = \begin{pmatrix} h_Z \\ 0 \\ 0 \end{pmatrix}, \tag{10}$$

$$\vec{h}_{+X} = \begin{pmatrix} h_{+X} \sin\theta_{+X} \cos\phi_{+X} \\ h_{+X} \sin\theta_{+X} \sin\phi_{+X} \\ h_{+X} \cos\theta_{+X} \end{pmatrix}, \tag{11}$$

$$\vec{h}_{-X} = \begin{pmatrix} -h_{-X} \sin\theta_{-X} \cos\phi_{+X} \\ h_{-X} \sin\theta_{-X} \sin\phi_{+X} \\ h_{-X} \cos\theta_{-X} \end{pmatrix}. \tag{12}$$

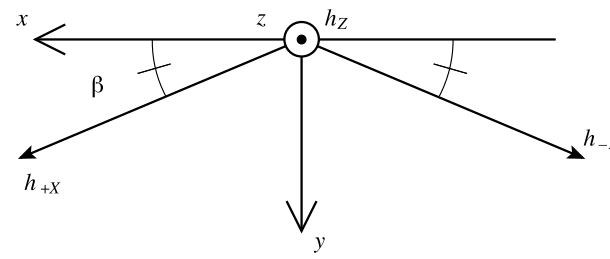

Figure 3. The antenna frame. The $\vec{z}$ axis is along the $\vec{h}_Z$ antenna direction. Here $\vec{x}$ and $\vec{y}$ are chosen so that the $\vec{h}_{+X}$ and $\vec{h}_{-X}$ antennas have supplementary azimuths. The $\vec{h}_{+X}$ and $\vec{h}_{-X}$ antenna colatitudes need not to be the same.

[11] In this particular frame, we can derive easily the source direction from the measurements. The useful expressions are A_{ZZ}, C^r_{+XZ}, C^i_{+XZ}, C^r_{-XZ}, C^i_{-XZ}, which are then written:

$$A_{ZZ} = \frac{Sh_Z^2}{2}\left[(1+Q)\sin^2\theta\right] \tag{13}$$

$$\begin{aligned} C^r_{+XZ} = \frac{Sh_{+X}h_Z}{2}[&(1+Q)(\cos\theta_{+X}\sin\theta \\ &- \sin\theta_{+X}\cos\theta\cos(\phi-\phi_{+X}))\sin\theta \\ &- U\sin\theta\sin\theta_{+X}\sin(\phi-\phi_{+X})] \end{aligned} \tag{14}$$

$$C^i_{+XZ} = \frac{-Sh_{+X}h_Z}{2}V\sin\theta\sin\theta_{+X}\sin(\phi-\phi_{+X}) \tag{15}$$

$$\begin{aligned} C^r_{-XZ} = \frac{Sh_{-X}h_Z}{2}[&(1+Q)(\cos\theta_{-X}\sin\theta \\ &+ \sin\theta_{-X}\cos\theta\cos(\phi+\phi_{+X}))\sin\theta \\ &+ U\sin\theta\sin\theta_{-X}\sin(\phi+\phi_{+X})] \end{aligned} \tag{16}$$

$$C^i_{-XZ} = \frac{Sh_{-X}h_Z}{2}V\sin\theta\sin\theta_{-X}\sin(\phi+\phi_{+X}) \tag{17}$$

Hence the colatitude and azimuth of the source direction are given by:

$$\tan\phi = \frac{h_{+X}\sin\theta_{+X}C^i_{-XZ} - h_{-X}\sin\theta_{-X}C^i_{+XZ}}{h_{+X}\sin\theta_{+X}C^i_{-XZ} + h_{-X}\sin\theta_{-X}C^i_{+XZ}}\tan\phi_{+X} \tag{18}$$

and

$$\tan\theta = \frac{A_{ZZ}h_{+X}h_{-X}\sin\theta_{+X}\sin\theta_{-X}\sin(2\phi_{+X})}{(h_{+X}A_{ZZ}\cos\theta_{+X} - h_Z C^r_{+XZ})h_{-X}\sin\theta_{-X}\sin(\phi+\phi_{+X}) + (h_{-X}A_{ZZ}\cos\theta_{-X} - h_Z C^r_{-XZ})h_{+X}\sin\theta_{+X}\sin(\phi-\phi_{+X})} \tag{19}$$

[12] As the tangent function is defined over an interval of π, we must have an initial guess value for the azimuth ϕ (an ephemeris coordinate of the observed object, for instance). There is no such need for the colatitude θ which is already defined over an interval of π.

[13] The azimuth ϕ is obtained from the imaginary parts of cross correlations. When $V = 0$ equation (18) is thus undefined and ϕ cannot be computed. This case deserves thus a specific treatment, which is discussed in section 2.1.2.

[14] All the wave parameters could be computed within the antenna frame but as the U and Q Stokes parameters depends on the orientation of the frame [see *Kraus*, 1966; *Hamaker and Bregman*, 1996], we choose to compute the wave Stokes parameters in the so-called wave frame, fixed relative to the radio source studied. The wave frame is defined as follows: $\vec{Z}_w$ is the normalized $\vec{k}$ vector of the incoming wave; we choose $\vec{Y}_w$ in the plane containing $\vec{k}$ and a typical axis of the observed object appropriate to the study (for instance the rotational or magnetic axis of the observed planet, with orientation along the south-north direction); the $\vec{X}_w$ axis completes the right hand triad. Geometry of this wave frame relative to the spacecraft frame is illustrated in Figure 2.

[15] Knowledge of the antennas directions (θ_n, ϕ_n) and of the source direction (θ, ϕ) implies that the parameters Ω_n and Ψ_n are known. The set of equations becomes thus a linear system with respect to the Stokes parameters and can be solved algebraically. We can retrieve the four Stokes parameters from each single two-antenna data set. In the following equations, the "±" index represents the pair of antenna used for the computation ($+XZ$ or $-XZ$). When Ω_n and Ψ_n are known, the correlations can be written in terms of a product of matrices:

$$\begin{bmatrix} A_{ZZ} \\ (h_Z/h_{\pm X})^2 & A_{\pm XX} \\ (h_Z/h_{\pm X}) & C^r_{\pm XZ} \\ (h_Z/h_{\pm X}) & C^i_{\pm XZ} \end{bmatrix} = \mathcal{M}\cdot\frac{Sh_Z^2}{2}\begin{bmatrix} 1 \\ Q \\ U \\ V \end{bmatrix}, \tag{20}$$

with

$$\mathcal{M} = \begin{bmatrix} \Omega_Z^2+\Psi_Z^2 & \Omega_Z^2-\Psi_Z^2 & 2\Omega_Z\Psi_Z & 0 \\ \Omega_{\pm X}^2+\Psi_{\pm X}^2 & \Omega_{\pm X}^2-\Psi_{\pm X}^2 & 2\Omega_{\pm X}\Psi_{\pm X} & 0 \\ \Omega_Z\Omega_{\pm X}+\Psi_Z\Psi_{\pm X} & \Omega_Z\Omega_{\pm X}-\Psi_Z\Psi_{\pm X} & \Omega_{\pm X}\Psi_Z+\Omega_Z\Psi_{\pm X} & 0 \\ 0 & 0 & 0 & -\Omega_{\pm X}\Psi_Z+\Omega_Z\Psi_{\pm X} \end{bmatrix} \tag{21}$$

This system can be solved when the matrix $\mathcal{M}$ is not singular. The determinant of $\mathcal{M}$ is:

$$\det(\mathcal{M}) = -2(\Omega_{\pm X}\Psi_Z - \Omega_Z\Psi_{\pm X})^4 \tag{22}$$

When $\det(\mathcal{M}) \neq 0$ we can find the Stokes parameters' vector:

$$\frac{Sh_Z^2}{2}\begin{bmatrix} 1 \\ Q \\ U \\ V \end{bmatrix} = \mathcal{M}^{-1}\cdot\begin{bmatrix} A_{ZZ} \\ (h_Z/h_{\pm X})^2 & A_{\pm XX} \\ (h_Z/h_{\pm X}) & C^r_{\pm XZ} \\ (h_Z/h_{\pm X}) & C^i_{\pm XZ} \end{bmatrix}. \tag{23}$$

with

$$\mathcal{M}^{-1} = \frac{\begin{bmatrix} \frac{\Omega_{\pm X}^2+\Psi_{\pm X}^2}{2(\Omega_{\pm X}\Psi_Z-\Omega_Z\Psi_{\pm X})} & \frac{\Omega_Z^2+\Psi_Z^2}{2(\Omega_{\pm X}\Psi_Z-\Omega_Z\Psi_{\pm X})} & -\frac{\Omega_{\pm X}\Omega_Z+\Psi_{\pm X}\Psi_Z}{\Omega_{\pm X}\Psi_Z-\Omega_Z\Psi_{\pm X}} & 0 \\ -\frac{\Omega_{\pm X}^2-\Psi_{\pm X}^2}{2(\Omega_{\pm X}\Psi_Z-\Omega_Z\Psi_{\pm X})} & -\frac{\Omega_Z^2-\Psi_Z^2}{2(\Omega_{\pm X}\Psi_Z-\Omega_Z\Psi_{\pm X})} & \frac{\Omega_{\pm X}\Omega_Z-\Psi_{\pm X}\Psi_Z}{\Omega_{\pm X}\Psi_Z-\Omega_Z\Psi_{\pm X}} & 0 \\ -\frac{\Omega_{\pm X}\Psi_{\pm X}}{\Omega_{\pm X}\Psi_Z-\Omega_Z\Psi_{\pm X}} & -\frac{\Omega_Z\Psi_Z}{\Omega_{\pm X}\Psi_Z-\Omega_Z\Psi_{\pm X}} & \frac{\Omega_{\pm X}\Psi_Z+\Omega_Z\Psi_{\pm X}}{\Omega_{\pm X}\Psi_Z-\Omega_Z\Psi_{\pm X}} & 0 \\ 0 & 0 & 0 & -1 \end{bmatrix}}{\Omega_{\pm X}\Psi_Z - \Omega_Z\Psi_{\pm X}}. \tag{24}$$

[16] Alternately, the latter system of equation can be formulated explicitly, in the antenna frame (where $\Psi_Z = 0$) for $S_\pm$ and $V_\pm$:

$$S_\pm = \frac{A_{\pm XX}h_Z^2\Omega_Z^2 - 2C_{\pm XZ}^r h_{\pm X}\Omega_{\pm X}h_Z\Omega_Z + A_{ZZ}h_{\pm X}^2\left(\Omega_{\pm X}^2+\Psi_{\pm X}^2\right)}{h_Z^2\Omega_Z^2h_{\pm X}^2\Psi_{\pm X}^2} \tag{25}$$

$$V_\pm = \frac{2C_{\pm XZ}^i}{S_\pm h_Z\Omega_Z h_{\pm X}\Psi_{\pm X}} \tag{26}$$

and in any frame (antenna, spacecraft or wave frame) for $Q_\pm$ and $U_\pm$:

$$U_\pm = \frac{A_{ZZ}h_{\pm X}^2\left(\Omega_{\pm X}^2-\Psi_{\pm X}^2\right) - A_{\pm XX}h_Z^2\left(\Omega_Z^2-\Psi_Z^2\right)}{S_\pm h_{\pm X}^2h_Z^2(\Omega_{\pm X}\Omega_Z+\Psi_{\pm X}\Psi_Z)(\Psi_Z\Omega_{\pm X}-\Psi_{\pm X}\Omega_Z)} - \frac{\Psi_Z\Omega_{\pm X}+\Psi_{\pm X}\Omega_Z}{\Omega_{\pm X}\Omega_Z+\Psi_{\pm X}\Psi_Z} \tag{27}$$

$$Q_\pm = \frac{2\left(A_{\pm XX}h_Z^2\Omega_Z\Psi_Z - A_{ZZ}h_{\pm X}^2\Omega_{\pm X}\Psi_{\pm X}\right)}{S_\pm h_{\pm X}^2h_Z^2(\Omega_{\pm X}\Omega_Z+\Psi_{\pm X}\Psi_Z)(\Psi_Z\Omega_{\pm X}-\Psi_{\pm X}\Omega_Z)} - \frac{\Omega_{\pm X}\Omega_Z-\Psi_{\pm X}\Psi_Z}{\Omega_{\pm X}\Omega_Z+\Psi_{\pm X}\Psi_Z} \tag{28}$$

We present separately the cases of $S_\pm$, $V_\pm$ and of $Q_\pm$, $U_\pm$ as the latter depend on the orientation of the frame while the former do not. $S_\pm$ and $V_\pm$ are derived in the antenna frame because equations (13) to (17) are easier to invert in this frame.

2.1.2. Case of a Purely Circularly Polarized Wave

[17] As seen above, the general inversion does not work when the imaginary parts of cross correlations are both zero. This occurs when $\theta = 0$ or π, or $V = 0$. The case $\theta = 0$ or π can be solved in the general case: the azimuth is then undefined and equation 19 gives the correct colatitude. The case $V = 0$ leads to an undetermination except if we also have $U = 0$ and $Q = 0$, i.e. if the wave is not polarized. In this section we study the case of a purely circularly polarized incoming wave. The case $V = 0$ is included in this assumption. It does have a practical interest because many radio emissions are unpolarized: solar type 3 bursts [*Dulk et al.*, 1998], lightning radio signatures (SED, i.e. Saturnian Electrical Discharges [*Zarka and Pedersen*, 1983]), etc.

[18] Within the antenna frame, the expressions of correlations induced by a purely circularly polarized incoming wave read:

$$A_{ZZ} = \frac{Sh_Z^2}{2}\sin^2\theta \tag{29}$$

$$A_{+XX} = \frac{Sh_{+X}^2}{2}\left[\left(\cos\theta_{+X}\sin\theta - \sin\theta_{+X}\cos\theta\cos\left(\phi-\phi_{+X}\right)\right)^2 + \left(\sin\theta_{+X}\sin\left(\phi-\phi_{+X}\right)\right)^2\right] \tag{30}$$

$$A_{-XX} = \frac{Sh_{-X}^2}{2}\left[\left(\cos\theta_{-X}\sin\theta + \sin\theta_{-X}\cos\theta\cos\left(\phi+\phi_{+X}\right)\right)^2 + \left(\sin\theta_{-X}\sin\left(\phi+\phi_{+X}\right)\right)^2\right] \tag{31}$$

$$C_{+XZ}^r = \frac{Sh_{+X}h_Z}{2}\left(\cos\theta_{+X}\sin\theta - \sin\theta_{+X}\cos\theta\cos\left(\phi-\phi_{+X}\right)\right)\sin\theta \tag{32}$$

$$C_{+XZ}^i = -\frac{Sh_{+X}h_Z}{2}V\sin\theta\sin\theta_{+X}\sin\left(\phi-\phi_{+X}\right) \tag{33}$$

$$C_{-XZ}^r = \frac{Sh_{-X}h_Z}{2}\left(\cos\theta_{-X}\sin\theta + \sin\theta_{-X}\cos\theta\cos\left(\phi+\phi_{+X}\right)\right)\sin\theta \tag{34}$$

$$C_{-XZ}^i = \frac{Sh_{-X}h_Z}{2}V\sin\theta\sin\theta_{-X}\sin\left(\phi+\phi_{+X}\right) \tag{35}$$

We are left with four unknowns (S, V, θ and ϕ). We introduce the quantities B_+ and B_-:

$$B_{+X} = A_{+XX} - \frac{\left(C_{+XZ}^r\right)^2}{A_{ZZ}} = \frac{Sh_{+X}^2}{2}\sin^2\theta_{+X}\sin^2\left(\phi-\phi_{+X}\right) \tag{36}$$

$$B_{-X} = A_{-XX} - \frac{\left(C_{-XZ}^r\right)^2}{A_{ZZ}} = \frac{Sh_{-X}^2}{2}\sin^2\theta_{-X}\sin^2\left(\phi+\phi_{+X}\right). \tag{37}$$

These expressions can be normalized as:

$$\tilde{B}_{+X} = 2B_{+X}/\left(h_{+X}^2\sin^2\theta_{+X}\right) \tag{38}$$

$$\tilde{B}_{-X} = 2B_{-X}/\left(h_{-X}^2\sin^2\theta_{-X}\right) \tag{39}$$

Combining them we obtain:

$$\tilde{B}_{+X} + \tilde{B}_{-X} = S\left(1 - \cos 2\phi \cos 2\phi_{+X}\right) \quad (40)$$

$$\tilde{B}_{+X} - \tilde{B}_{-X} = S\left(-\sin 2\phi \sin 2\phi_{+X}\right) \quad (41)$$

This leads to:

$$\cos 2\phi \cos 2\phi_{+X} - \frac{\tilde{B}_{+X} + \tilde{B}_{-X}}{\tilde{B}_{+X} - \tilde{B}_{-X}} \sin 2\phi \sin 2\phi_{+X} = 1 \quad (42)$$

which is solved introducing Θ as:

$$\tan 2\Theta = \left(\tilde{B}_{+X} + \tilde{B}_{-X}\right) / \left(\tilde{B}_{+X} - \tilde{B}_{-X}\right) \tan 2\phi_{+X}. \quad (43)$$

Notice that even if 2Θ is defined over 2π, there is a π indetermination on Θ. The latter equation implies:

$$\cos[2(\phi + \Theta)] = \frac{\cos 2\Theta}{\cos 2\phi_{+X}} \quad (44)$$

and we finally obtain the azimuth ϕ as:

$$\phi = \frac{\varepsilon_1}{2} \arccos\left(\frac{\cos 2\Theta}{\cos 2\phi_{+X}}\right) - \Theta + \varepsilon_2 \pi \quad (45)$$

where $\varepsilon_1 \in \{-1,1\}$ and $\varepsilon_2 \in \{0,1\}$. An ephemeris initial guess is needed to discriminate between these four solutions.

[19] The flux S is computed from ϕ, $\tilde{B}_{+X}$ and $\tilde{B}_{-X}$:

$$S = \tilde{B}_{+X} + \tilde{B}_{-X} - \frac{\tilde{B}_{+X} - \tilde{B}_{-X}}{\tan 2\phi \tan 2\phi_{+X}} \quad (46)$$

and the colatitude θ from S and $A_{ZZ(\pm)}$ (the last $\pm$ index refers to pair of antenna from which the A_{ZZ} autocorrelation comes):

$$\theta_{\pm} = \arcsin\left[\left(\frac{2A_{ZZ(\pm)}}{Sh_Z^2}\right)^{1/2}\right]. \quad (47)$$

The real colatitude can be either $\theta_{\pm}$ or $\pi - \theta_{\pm}$. The resulting source position angles $\theta_{\pm}$ and ϕ have thus to be compared with ephemeris data as in the general case to remove all angular indeterminations. Note that in this particular inversion, the angular indeterminations are not just the two opposite directions indetermination, which is inherent to any DF inversion. This method must then be used with care and on precise ephemeris data.

[20] Finally, the degree of circular polarization V is obtained through:

$$V_{\pm} = \frac{\mp C^i_{\pm XZ}}{\sqrt{A_{\pm XX} A_{ZZ(\pm)} - \left(C^r_{\pm XZ}\right)^2}} \quad (48)$$

The source colatitude $\theta_{\pm}$ and the degree of circular polarization $V_{\pm}$ can be computed with either two-antenna data sets of the three-antenna data set.

2.1.3. Partial Inversions With Two-Antenna Data Sets

[21] The two inversions discussed in this section are not full DF inversions as they only retrieve partial information on the wave, assuming some wave parameters to be known. These partial inversions are useful when the receiver is not in the specific DF mode (i.e. on Cassini, when RPWS is not switching between the ($+X$, Z) and ($-X$, Z) pairs of monopoles). Additionally, in case of the loss of one of the $\pm X$ monopoles, these partial inversions will be the only inversions applicable to the data. In the dipole mode for instance, the $+X$ and $-X$ monopoles antennas are connected to a single terminal and used as a dipole D together with the monopole Z on the 2nd channel. We can also apply a partial inversion when the two successive autocorrelations A_{ZZ} of a three-antenna data set are significantly different (this means that the emission has changed between the two ($+X$, Z) and ($-X$, Z) successive measurements).

[22] The two partial inversions to be considered are:

2.1.3.1. Polarimeter Mode

[23] If the position of the source is known (e.g., very far from a planet, when its radio sources can be considered to coincide with the planet's center), we can retrieve the four Stokes parameters by using the same inversion technique as used in the general DF analytical inversion (see section 2.1.1), but skipping the source direction determination steps.

2.1.3.2. Circular Polarization Mode

[24] In case of a purely circularly polarized wave, the Stokes parameters U and Q which describe the linear polarization are zero. An analytical inversion in then possible on two-antenna data sets [*Lecacheux*, 2000]. This inversion solves the system for S, V, θ and ϕ. It can also be used when $V = 0$. When the receiver is in DF mode (i.e., using three-antenna data sets), the method presented in section 2.1.2 can be more robust (by combining together more measurements) if the source parameters (especially the flux S) do not vary between the two successive two-antenna data sets. However, as discussed earlier, the angular indeterminations of the three-antenna method (see section 2.1.2) can also be a problem which can be solved by using the present two-antenna inversion.

2.2. Antenna Calibration

[25] The physical parameters (length and orientation) of the antennas are known by construction. Those parameters would be identical to the electrical axes if the antennas were real short dipoles isolated in space (i.e., not perturbed by the conducting spacecraft structure). "Short" means that the electric field of an incom-

ing wave is spatially homogeneous over the antenna length. The voltage induced by this electric field $\vec{E}$ can thus be written: $V = \vec{h}.\vec{E}$ where $\vec{h}$ is the effective antenna vector. This is the case if $2h \ll \lambda/2$ (i.e., $2h \lesssim \lambda/10$). Above the first antenna resonance ($h = \lambda/4$), the antenna pattern becomes multilobed and the effective length becomes complex [*Ortega-Molina and Daigne*, 1984]. Using a wire grid model, Fischer [*Fischer et al.*, 2003; *Fischer and Macher*, 2004] showed that in the case of the Cassini/RPWS antennas the short antenna hypothesis upper frequency limit was at about 1.5 MHz. This frequency limit is equivalent to the following condition: $2h < \lambda/10$. The inversions presented here can only be applied when the short dipole hypothesis is valid.

[26] In the case of Cassini/RPWS, the antennas are monopoles. A monopole is equivalent to a dipole if it is made of straight conducting wire against an infinite conducting plane perpendicular to the wire direction. The real RPWS antennas are 10 m monopoles (actually tubular conducting booms) placed in front of a nonplanar conducting surface whose dimensions are roughly 4 × 12 m. We assume that for $f \lesssim 1$ MHz we can find an equivalent set of electrical dipoles to this set of monopole antennas. We present here an analytical way to solve the equations of system (1)–(7) for antenna parameters. This process is called the antenna calibration. A first antenna calibration has been made by *Rucker et al.* [1996], using a rheometric analysis on a scaled model (1/30th) of the Cassini spacecraft.

[27] The rheometric analysis consists of measuring the antenna responses on a scaled model of the spacecraft immersed in a tank filled with a dielectric medium (water in the case of the Cassini model rheometry) [*Rucker et al.*, 1996]. A static electric field is imposed in the tank. The static field induces a voltage $V = \vec{h}.\vec{E}$ on the antenna, similarly to the voltage induced in the short dipole hypothesis. The antenna response is measured in function of the model orientation. The electric antenna direction is given by the zero-response direction ($\vec{h} \perp \vec{E}$) or by the maximum-response direction ($\vec{h}//\vec{E}$). The effective antenna length is also retrieved, but the numbers are not reliable because of the poor modelization of the antenna feed and fixation (which defines the antenna base capacitance).

[28] The antenna response of a short electrical dipole of length L is proportional $L \sin^2\theta$, where θ is the source colatitude (with respect to the antenna direction). This implies that determining the antenna length is best done when $\theta \sim 90°$ (maximum response). The antenna lengths will thus be calibrated for source antenna configuration for which $45° \lesssim \theta \lesssim 135°$. When $\theta \approx 0$ or 180°, the antenna response is highly sensitive to θ. The antenna angles will thus be calibrated when $\theta \lesssim 45°$ or $\theta \gtrsim 135°$. As those geometrical configurations are mutually exclusive, we will calibrate first the antenna lengths and then the antenna directions using different source antenna configurations. Moreover, each antenna direction can be calibrated separately as the angular separation between any two antennas is ~90°.

[29] The analytical calibration inversion presented below assumes purely circularly polarized emissions (i.e., $U = 0$ and $Q = 0$). This choice is justified by the fact that: (1) the system of equations can be inverted in that case with two-antenna data sets, and (2) the calibration of Cassini/RPWS has been carried out using the circularly polarized jovian HOM emissions [*Ortega-Molina and Lecacheux*, 1991; *Vogl et al.*, 2004].

[30] In the wave frame (Figure 2), a purely circularly polarized wave induces the following responses of the receiver:

$$A_{XX} = 1/2\, S h_X^2 \sin^2\theta_X \tag{49}$$

$$A_{ZZ} = 1/2\, S h_Z^2 \sin^2\theta_Z \tag{50}$$

$$C^r_{XZ} = 1/2\, S h_X h_Z \sin\theta_X \sin\theta_Z \cos(\phi_X - \phi_Z) \tag{51}$$

$$C^i_{XZ} = -1/2\, S V h_X h_Z \sin\theta_X \sin\theta_Z \sin(\phi_X - \phi_Z) \tag{52}$$

Note that the X index represents either the $+X$, $-X$ or D, depending the antenna pair involved in the two-antenna data set. In case of antenna length calibration, we solve the system for h_X/h_Z. In case of antenna direction calibration, we solve it for θ_i and ϕ_i (with $i \in \{X, Z\}$). Additionally, in that case, we can compute V and S.

2.2.1. Antenna Lengths

[31] Combining equations (49) and (50), we get:

$$h_Z/h_X = \sqrt{\frac{A_{ZZ}}{A_{XX}} \frac{\sin^2\theta_X}{\sin^2\theta_Z}} \tag{53}$$

This equation gives the antenna ratios h_Z/h_{+X}, h_Z/h_{-X} or h_Z/h_D, depending on the antennas pair used for the measurement. It is not possible to obtain absolute antenna lengths with DF measurements, as they always appear in a product Sh^2 with S a priori unknown (Jovian radio flux density is very sporadic). Approximate lengths can be estimated from the frequency of the first resonance observed or from the analysis of observations of a radio source of known flux density (as the galactic background noise) [see *Zarka et al.*, 2004].

2.2.2. Antenna Directions

[32] With our assumptions, a set of four unknowns remains to be determined: S, V, θ_i and ϕ_i (with $i \in \{+X, -X, D, Z\}$ depending on which antenna we are calibrat-

ing). The flux intensity S cannot be isolated from a squared antenna length in the present inversion. Hence we only retrieve Sh_Z^2 (the h_Z antenna length has been arbitrarily chosen as a reference length).

[33] The Z antenna is calibrated as follows:

$$\theta_Z = \frac{\pi}{2} + \varepsilon_\theta \left[\frac{\pi}{2} - \arcsin\left(\sqrt{\frac{A_{ZZ}}{A_{XX}} \frac{h_X^2}{h_Z^2} \sin^2 \theta_X} \right) \right] \quad (54)$$

$$\phi_Z = \phi_X + \varepsilon_\phi \arccos\left(\frac{C_{XZ}^r}{\sqrt{A_{ZZ} A_{XX}}} \right) \quad (55)$$

$$Sh_Z^2 = \frac{h_Z^2}{h_X^2} \frac{2A_{XX}}{\sin^2 \theta_X} \quad (56)$$

$$V = \frac{-\varepsilon_\phi C_{XZ}^i}{\sqrt{A_{ZZ} A_{XX} - (C_{XZ}^r)^2}} \quad (57)$$

where $\varepsilon_\theta = \text{sign}(\theta_Z^0 - \pi/2)$ and $\varepsilon_\phi = \text{sign}(\phi_Z^0 - \phi_X)$ with $\phi_Z^0 - \phi_X \in [-\pi, \pi]$. Those two last expressions require an initial guess for the antenna direction defined by its colatitude θ_Z^0 and azimuth ϕ_Z^0, which can be the physical or the rheometrical value [see *Rucker et al.*, 1996] (we do not expect the electrical dipole direction to be far from those directions). The Z antenna orientation derived here is in the wave frame, so it has to be rotated back in the spacecraft frame or in any other relevant frame.

[34] The X antenna is calibrated in the same way:

$$\theta_X = \frac{\pi}{2} + \varepsilon_\theta \left[\frac{\pi}{2} - \arcsin\left(\sqrt{\frac{A_{XX}}{A_{ZZ}} \frac{h_Z^2}{h_X^2} \sin^2 \theta_Z} \right) \right] \quad (58)$$

$$\phi_X = \phi_Z - \varepsilon_\phi \arccos\left(\frac{C_{XZ}^r}{\sqrt{A_{ZZ} A_{XX}}} \right) \quad (59)$$

$$Sh_Z^2 = \frac{2A_{ZZ}}{\sin^2 \theta_Z} \quad (60)$$

$$V = \frac{\varepsilon_\phi C_{XZ}^i}{\sqrt{A_{ZZ} A_{XX} - (C_{XZ}^r)^2}} \quad (61)$$

with similar definitions for ε_θ and ε_ϕ definitions. The same remarks as for the Z antenna calibration apply.

3. Error Analysis and Data Selection

[35] The DF inversions presented are analytical. Studying errors and their propagation is thus easy to carry out through simulations. Note that an analytical error propagation analysis has also been carried out (see Appendix A) but it will not be presented extensively in this paper.

[36] The different sources of error are: analytical indeterminations, digitization, signal to noise ratio (SNR), error on preset parameters and emission variation between two successive ($+X$, Z) and ($-X$, Z) two-antenna measurements. For each case we have carried out a forward modelling analysis (i.e., a complete simulation of modelized measurements exploring the whole space of unknowns parameters) to quantify the effect of the corresponding error. We have simulated a series of three-antenna data sets, covering the whole wave parameter space with convenient stepping for each type of error study. In case of SNR or digitization, we have computed a series of simulated measurements with variable flux, then we have applied the corresponding alteration to the simulated measurements and finally we applied the DF inversions on them. In case of preset parameters bias, we have computed a series of simulated measurements and we applied the DF inversions with an altered set of preset parameters. Each source of error has been isolated and simulated separately.

[37] Some useful angular distances have to be defined first:

[38] 1. Here α_i is the angular distance from the source direction to the ith electrical antenna direction ($i \in \{+X, -X, D, Z\}$).

[39] 2. Here β_{XZ} is the angular distance from the source direction to the (X, Z) electrical antenna plane, where $X \in \{+X, -X, D\}$.

3.1. Errors Affecting the DF Inversions

[40] Both DF inversions (general case and circular polarization case) have been studied and the same error analysis has been carried out: numerical errors, error on antenna parameters, digitization error, signal to noise ratio (SNR), changing in the emission between the two successive two-antenna data sets. We express the alteration of the results in terms of four quantities: the angular distance between the resulting and the input source position ($\delta\theta$), the difference between the resulting and input flux ($\delta S_\pm$), degree of linear polarization ($\delta L_\pm$, where $L_\pm = (U_\pm^2 + Q_\pm^2)^{1/2}$) and degree of circular polarization ($\delta V_\pm$). The results presented below have all been computed with the ($+X$, Z) pair of antennas. Similar results have been obtained for the ($-X$, Z) or (D, Z) pairs of antennas. All the results will be summarized in the end. We will first study the general case inversion and then the circular polarization case.

[41] Each simulation has been carried out with the following set of parameters.

[42] The source position is set as follows: the $n_\theta = 72$ steps for colatitude regularly distributed in the [0°, 180°] range, $n_\phi = 144$ steps for azimuth regularly

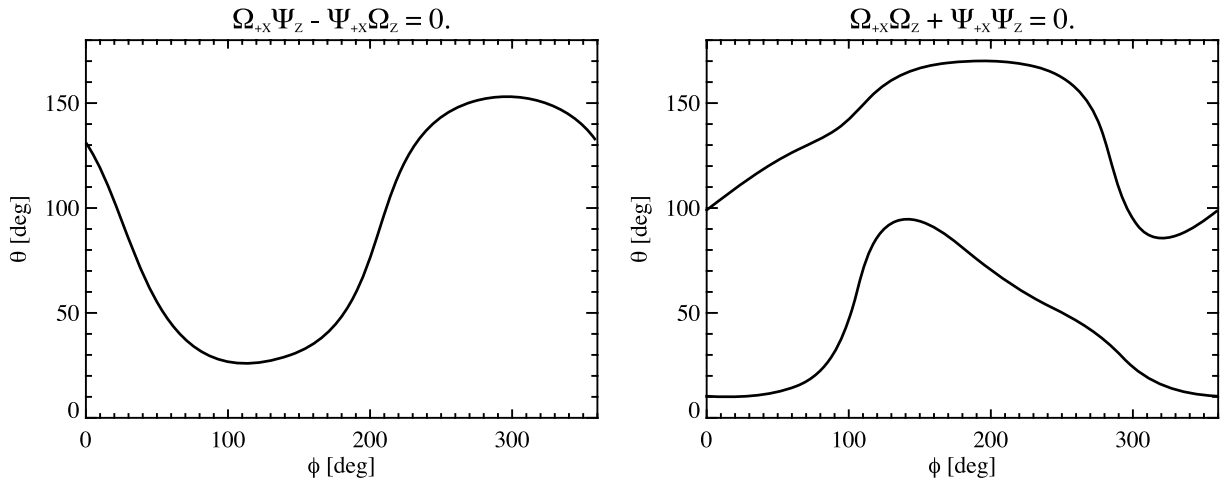

Figure 4. (left) The curve is the locus of the points for which $\Omega_{+X}\Psi_Z - \Psi_{+X}\Omega_Z = 0$. (right) The two curves are the locus of the points for which $\Omega_{+X}\Omega_Z + \Psi_{+X}\Psi_Z = 0$. The θ and ϕ coordinates are the colatitude and azimuth in the spacecraft frame. Those curves correspond to undetermined configurations in the general case DF analytical inversion.

distributed in the [0°, 360°] range. Additionally, the direction $\theta = 0°$ and $\theta = 180°$ are computed only once. Hence the total number of source positions is $n_{src} = 2 + (n_\theta - 1) \times n_\phi$.

[43] The input flux S is in general fixed to a single value as it is a multiplying factor in front of each simulated measurements. The 2 cases where a series of flux values are used are SNR and digitization noise simulations. A typical number is $S = 10^{-16}$ V^2/Hz, which corresponds to a 20 dB above background with a $\sigma = 5\ 10^{-18}$ V^2/Hz background noise level.

[44] Concerning the wave polarization, the Q, U and V degrees of polarization are distributed on the [−1,1] range, with a typical 0.2 spacing (11 values). Excluding all nonphysical degrees of polarization ($Q^2 + U^2 + V^2 > 1$), $n_{pol} = 515$ points (among 1331) remains.

[45] A typical simulation set of parameters is then composed of $n_{pol} \times n_{src} = 5266390$ points.

3.1.1. General Case Inversion

3.1.1.1. Analytical Indetermination

[46] Equation 18 is defined only when $V \neq 0$ and $\theta \neq 0$ or π. As seen above, the former is taken into account in the circular polarization case inversion and the latter is actually a solvable case. The second indetermination occurs when $\det(\mathcal{M}) = 0$ which is equivalent to:

$$\Omega_{+X}\Psi_Z - \Psi_{+X}\Omega_Z = 0 \tag{62}$$

This last relation is also equivalent to $\beta_{+XZ} = 0$, i.e., when the source direction lies in the (+X, Z) antenna plane. The geometrical configuration defined by equation 62 is the (+X, Z) antenna plane (see Figure 4, left plot). The matrix $\mathcal{M}$ (see equation (21)) is then singular so that only the position (θ, ϕ) of the source can be computed. A third indetermination occurs for:

$$\Omega_{\pm X}\Omega_Z + \Psi_{\pm X}\Psi_Z = 0 \tag{63}$$

(see equations (27) and (28)). In this later case, S and V can be computed accurately but neither U nor Q. The corresponding directions are displayed in Figure 4 (right plot).

3.1.1.2. Digitization

[47] These errors are introduced by the receiver. An Automatic Gain Control (AGC) loop permanently adjusts the voltage input level to the 32-bit digitization ramp. The digitized signals are then correlated to obtain the measurements which are compressed on 8-bit words, using a pseudolog coding. The dynamic of this whole system is 90 dB. Errors are introduced by the AGC at low level signals (the AGC is not linear when $S \lesssim 10^{-17}$ V^2/Hz) and by the 8-bit log compression on the whole dynamic range. We have simulated digitization errors based on the RPWS receiver characteristics. As the future STEREO/SWAVES receiver will have a similar AGC loop but with a 12-bit log compression, we have also carried out the simulations in this case.

[48] Figure 5 shows histograms of the error induced by digitization on the A_{ZZ} autocorrelation normalized to the flux intensity (taken here to be $S = 10^{-16}$ or 10^{-14} V^2/Hz). The width of the histogram is ∼0.01, which is equivalent to a ∼20 dB SNR value. Similar plots for other measurements (A_{XX}, C^r_{XZ} and C^i_{XZ}) show exactly the same dispersion. The flux intensity does not

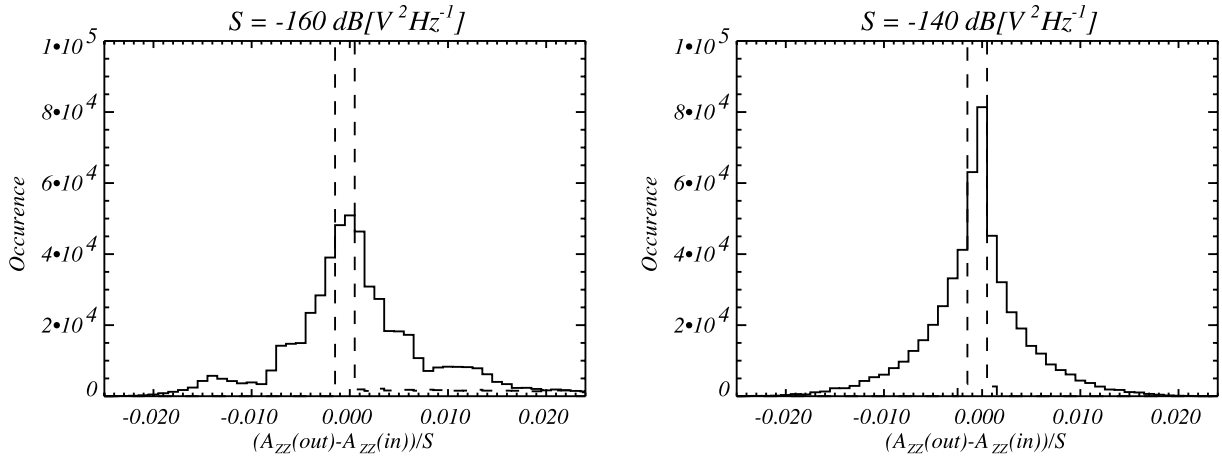

Figure 5. Histograms of the simulated A_{ZZ} dispersion caused by a RPWS-like digitization process. The dispersion is normalized to the input flux intensity (left) $S = 10^{-16}$ V^2/Hz and (right) 10^{-14} V^2/Hz. Plain line corresponds to an 8-bit digitization process and dashed ones to 12-bit. The total number of points for each simulation is 524,575 points.

change the histogram width except for $S \lesssim 10^{-16}$ V^2/Hz; such low intensity implies low measurement values that are out of the AGC linear range.

[49] Figure 6 shows the dispersion of DF results for the source position ($\delta\theta$), as induced by the digitization. The plots show $\delta\theta$ versus α_Z for two different simulated intensities ($S = 10^{-16}$ and 10^{-14} V^2/Hz). For low S ($\lesssim 10^{-16}$ V^2/Hz) and low α_Z (<30°), $\delta\theta$ can be as high as 90°. For higher flux intensities ($S \gg 10^{-16}$ V^2/Hz), the $\delta\theta$ envelope versus α_Z does not vary with S. Moreover $\delta\theta$ decreases with α_Z. Selecting source direction that corresponds to α_Z lower than a fixed $\alpha_Z^{\lim}$ value will improve the accuracy on the source position. For each angular selection, we compute the histogram of $\delta\theta$ (see Figure 7a) which gives the error probability level at 50% and 1% (i.e., the probability that the error exceeds that limit). Figure 7b shows the error probability levels (50% and 1%) versus the $\alpha_Z^{\lim}$ selection criterion. This Figure shows four series of points. The labels on the right side gives the corresponding error level probability for 8-bit and 12-bit digitization. For the 8-bit case, the figure shows that: (1) the probability to have errors higher than ~5° is 1%; (2) the probability to have errors lower than ~1° is 50%; (3) the probability to have errors lower than ~0.5° is 50% for $\alpha_Z^{\lim} < 30°$. Finally, comparing the results obtained with 8-bit and 12-bit digitization on Figure 7b, we observe that the error probability levels are separated by a factor ~16 which is $2^{12}/2^8$, as expected.

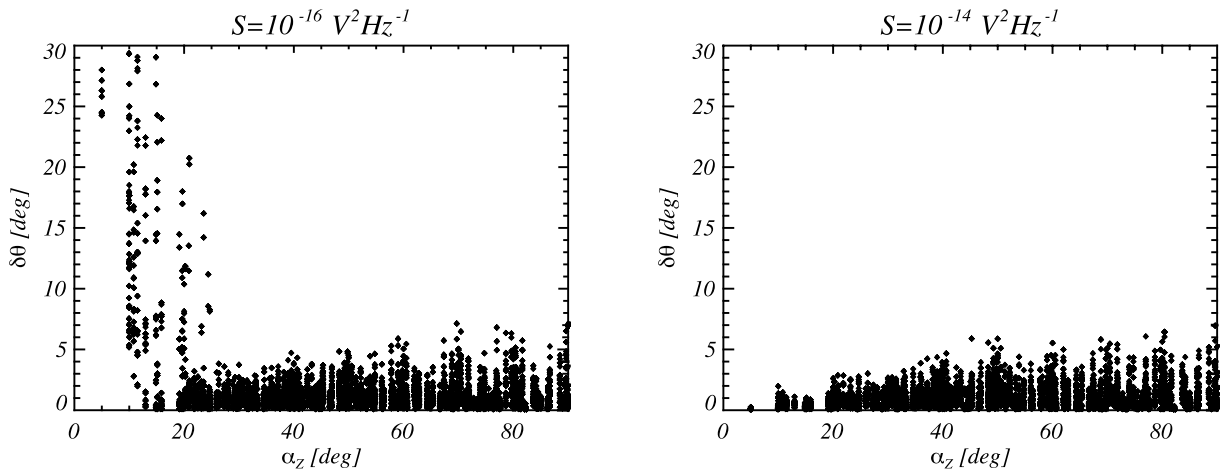

Figure 6. The $\delta\theta$ versus α_Z in case of RPWS-like (8-bit) digitization errors for two flux intensities (left) $S = 10^{-16}$ V^2/Hz and (right) 10^{-14} V^2/Hz.

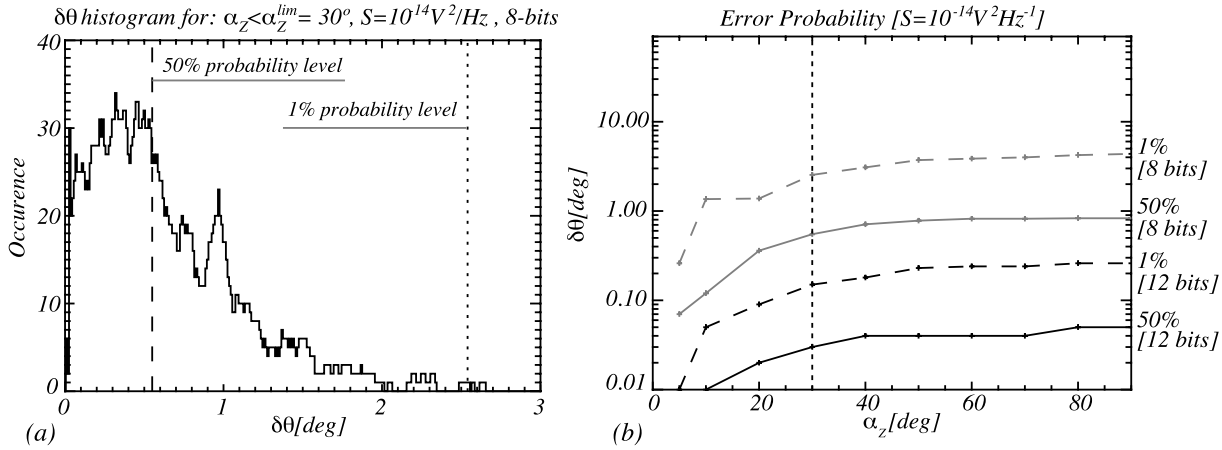

Figure 7. Error probability levels on the source position δθ caused by the digitization. (a) Histogram of δθ for $\alpha_Z < \alpha_Z^{\lim} = 30°$, $S = 10^{-14}$ V^2/Hz and a 8-bit digitization. The 50% and 1% probability levels are shown. (b) Error probability levels for different $\alpha_Z^{\lim}$ and 8-bit/12-bit digitization. The vertical dotted line corresponds to the results illustrated in Figure 7a.

[50] Figure 8 shows the DF results dispersion for flux (δS_+), linear and degree of circular polarization (δL_+ and δV_+) versus β_{+XZ}, which appears to be the relevant parameter here. The results shown are for the (+*X*, *Z*) pair of antennas inversion. The same results are obtained with (−*X*, *Z*) pair of antennas inversion. The plots show a high level dispersion at low β_{+XZ}. If $\beta_{\pm XZ} \sim 0$, $\delta S_\pm$ can be as high as 100 dB [V^2/Hz] and nonphysical degrees of polarization (>1) can be obtained. Selecting over β_{+XZ} improves the DF results: (1) $\beta_{+XZ} > 20°$ gives $\delta S_\pm < 1$ dB [V^2/Hz], $\delta L_\pm < 0.30$ and $\delta V_\pm < 0.10$; and (2) $\beta_{+XZ} > 40°$ gives $\delta S_\pm < 0.5$ dB [V^2/Hz], $\delta L_\pm < 0.10$ and $\delta V_\pm < 0.05$. Note that these results do not depend on the flux intensity *S*.

3.1.1.3. Signal to Noise Ratio

[51] The noise added to the autocorrelations is a Gaussian noise distribution with a width $\sigma = S_{bg}/\sqrt{B\tau}$ where S_{bg} is the background intensity level, *B* and τ the frequency bandwidth and integration time of the measurement. Note that we use background intensity level and not total intensity level to compute the noise width. This comes from the fact that we are using single measurements of the flux *S* and not a series of successive measurements. The uncertainty of the measurement is then the one of the level of the background intensity. The typical values for those parameters are $S_{bg} = 10^{-16}$ V^2/Hz, $B = 25$ kHz and $\tau = 16$ ms for typical measurements with RPWS. These values lead to $\sigma = 5\ 10^{-18}$ V^2/Hz. Note that the galactic background intensity is of the order of 10^{-16} to $3\ 10^{-14}$ V^2/Hz (depending of frequency) and the receiver noise level is as low as $2\ 10^{-16}$ V^2/Hz [*Zarka et al.*, 2004, Figures 4a–4b]. We have simulated measurements for four flux intensity levels $S = 5\ 10^{-17}$, $2.5\ 10^{-16}$, 10^{-15} and 10^{-14} V^2/Hz, corresponding respectively to SNRs of 10, 17, 23, and 33 dB.

[52] Figure 9 shows the error probability levels for different angular selections and different SNRs, using a similar method as for Figure 7. As the error probability

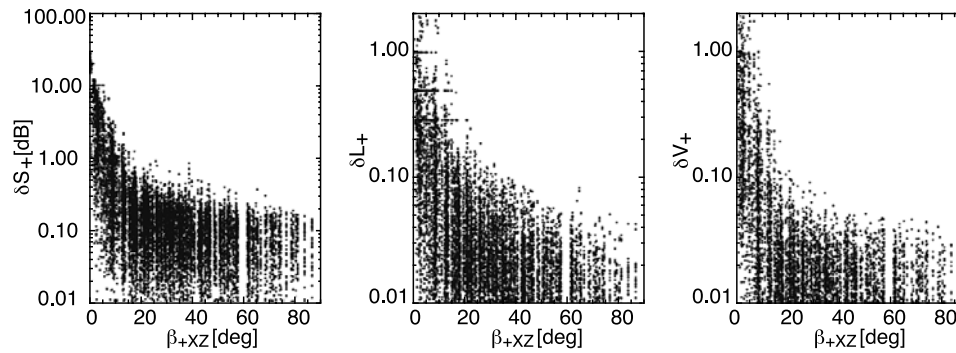

Figure 8. Shown are δS_+, δL_+, and δV_+ versus β_{+XZ} in case of RPWS-like digitization errors.

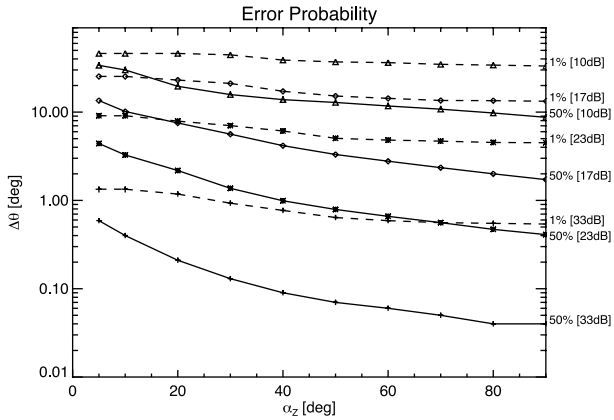

Figure 9. Error probability levels on the source position $\delta\theta$ caused by the SNR. The figure shows the errors probability levels for different $\alpha_Z^{\lim}$ and different SNRs: triangles, 10 dB; diamonds, 17 dB; crosses, 23 dB; pluses, 33 dB. Plain lines are for 50% error probability levels and dashed lines for 1% levels.

level increases when $\alpha_Z^{\lim}$ is getting closer to zero, the angular selections are $\alpha_Z > \alpha_Z^{\lim}$ in this case. In all cases, at $\alpha_Z \sim 0$ (i.e., when the source is in the Z antenna direction), $\delta\theta$ can be as high as 90°: (1) at 33 dB, the probability to have $\delta\theta < 1°$ is 50% for any $\alpha_Z^{\lim}$ and 1% for $\alpha_Z^{\lim} > 25°$; (2) at 2 dB, the probability to have $\delta\theta < 1°$ is 50% for $\alpha_Z^{\lim} > 40°$; for $\delta\theta < 2°$, the 50% level is reached for $\alpha_Z^{\lim} > 20°$; and for $\delta\theta < 5°$ the 50% level is reached for any $\alpha_Z^{\lim}$, the 1% level for $\alpha_Z^{\lim} > 60°$; (3) at 17 dB, $\delta\theta < 2°$ cannot be reached but the probability to have $\delta\theta < 5°$ is 50% for $\alpha_Z^{\lim} > 35°$; and (4) at 10 dB, no accurate source position measurements ($\delta\theta < 2°$) can be done.

[53] In summary, accurate source position measurements at a 50% error probability level (<2°) require a SNR $\gtrsim$ 20 dB and $\alpha_Z^{\lim} < 20°$. For a SNR $\gtrsim$ 30 dB, the source position accuracy is as low as $\delta\theta < 1°$ with a 50% probability (except for $\alpha_Z = 0$).

[54] Concerning the flux and polarization measurements accuracy, Table 1 summarizes the envelope of the clouds of points of Figure 8 (which corresponds well to the 1% error probability levels) for $\delta S_\pm$, $\delta L_\pm$ and $\delta V_\pm$, with a $\beta_{\pm XZ} > 20°$ angular selection. Flux measurements can be done with a 1 dB [V^2/Hz] accuracy for SNR as low as 17 dB, but no accurate polarization measurements can be done for SNR < 23 dB.

3.1.1.4. Preset Parameters Bias

[55] In case of errors on preset parameters (i.e., antenna calibration error in the general case DF inversion) there are two possible types of errors: on antenna effective length or on electric antenna direction.

[56] 1. Introducing a +10% bias on the Z antenna length: we find $\delta\theta_{\max} = 4.2°$. Figure 10a shows the bias induced on the source position. The region for which $\delta\theta < 2°$ has been hatched. (1) With no angular selection, we have $\delta S < 0.82$ dB [V^2/Hz], $\delta L_\pm < 0.11$ and $\delta V_\pm < 0.05$; and (2) selecting source positions for which $\alpha_Z < 40°$, we obtain $\delta S_\pm < 0.5°$, $\delta L_\pm < 0.06$ and $\delta V < 0.03$.

[57] 2. Introducing a +2° bias on the $+X$ antenna colatitude: The bias induced on the source position results is displayed on Figure 10b and is of the order of 1° in all directions, except in the hatched region. The other parameters are altered with deviations of $\delta S_\pm <$ 0.22 dB [V^2/Hz], $\delta L_\pm < 0.040$ and $\delta V_\pm < 0.015$ for all source positions.

3.1.1.5. Source Temporal Variability

[58] A last source of error is the variation of the wave parameters between two successive ($+X$, Z) and ($-X$, Z) two-antenna data sets used in the DF mode. In this particular mode, the Z antenna autocorrelation A_{ZZ} is measured twice (once in each two-antenna data sets). In practice, we compare the two values of A_{ZZ} to check if the emission did not significantly vary between the two successive two-antenna data sets. Many factors can lead to a variation in A_{ZZ} but it is most likely the flux S that will vary in case of planetary or solar radio emissions which are intrinsically sporadic.

[59] We have simulated a 10% increase of S between the 1st and 2nd two-antenna data sets. The resulting source position error is displayed on Figure 11b: the source positions for which we have $\delta\theta > 2°$ are hatched. The maximum value of $\delta\theta$ is $\delta\theta_{\max} = 6°$. For a 1% increase, errors are similar but 1 order of magnitude smaller, as seen on Figure 11a.

[60] Concerning the flux and polarization measurements, taking $\beta_{\pm XZ} > 20°$ leads to the following accuracy: $\delta S_\pm < 1$ dB [V^2/Hz], $\delta L_\pm < 0.12$ and $\delta V_\pm < 0.06$. Note that the angular selection defined in Figure 11 is totally incompatible with $\beta_{\pm XZ} > 20°$. Taking $\Delta A_{ZZ} < 1\%$ will ensure that errors are lower than $\delta\theta < 0.6°$, $\delta S_\pm < 0.1$ dB [V^2/Hz], $\delta L_\pm < 0.02$ and $\delta V_\pm < 0.01$.

[61] In summary, with antenna directions known with an accuracy of 2° and effective length with a 1% accuracy, we obtain a maximum error of 1° on the source position (with a 50% error probability level). With a

Table 1. One-Percent Error Probability Levels for $\delta S_\pm$, $\delta L_\pm$, and $\delta V_\pm$, With a $\beta_{\pm XZ} > 20°$ Angular Selection[a]

SNR, dB	$\delta S_\pm$ [dB (V^2/Hz)]	$\delta L_\pm$, %	$\delta V_\pm$, %
10	2.0	$\gg$100	$\gg$100
17	1.0	100	100
23	0.15	10	2
33	$\ll$0.1	1	$\ll$1

[a]Flux intensities are measured accurately ($\delta S_\pm < 1$ dB [V^2/Hz]) for SNR > 17 dB. Polarization measurements are accurate (<10%) for SNR > 23 dB. Note that nonphysical degrees of polarization may be found for SNR $\lesssim$ 17 dB.

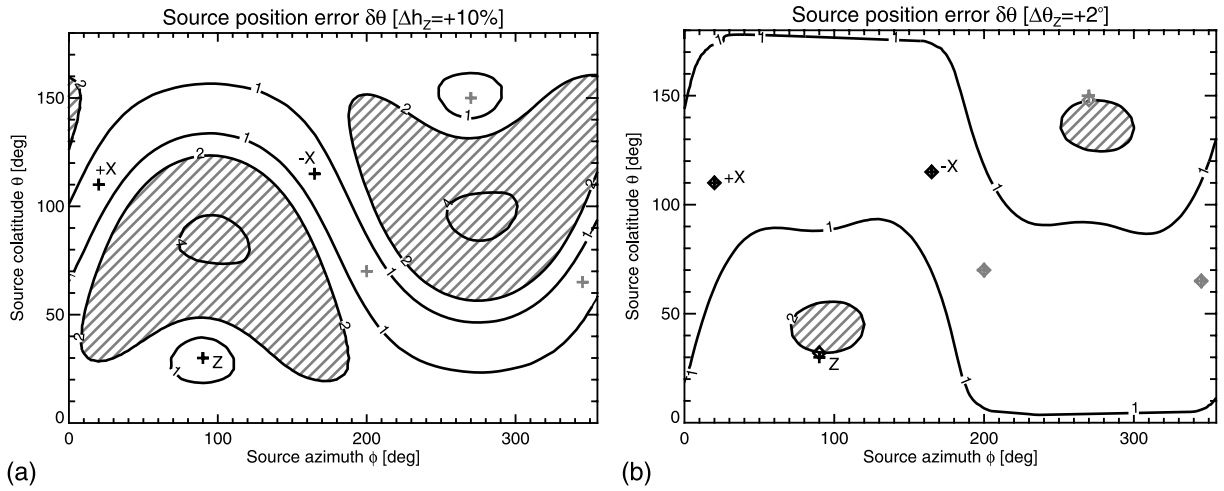

Figure 10. Error on the source position $\delta\theta$ introduced by (a) a +10% bias on the Z antenna length h_Z, and (b) a +2° bias on the Z antenna colatitude θ_Z. Coordinates are in the spacecraft frame. The region in which $\delta\theta > 2°$ has been hatched. The crosses and the diamonds represent, respectively, the input and biased the antenna directions. Boldface symbols correspond to the antenna direction, lightface ones to the opposite directions. Lines are isocontours in degree.

selection on the source position, $\beta_{\pm XZ} > 20°$, we obtain $\delta S_\pm < 1.0$ dB [V^2/Hz], $\delta L_\pm < 0.10$ and $\delta V_\pm < 0.10$. All the error analysis results for the general case DF inversion are displayed in Table 2, and summarized in Table 3.

3.1.2. Circular Polarization Inversion

[62] Circular polarization inversion In this case, errors occur mainly in the Z antenna direction and in the plane perpendicular to the Z antenna, see equations (36), (37) and (47). The results are summarized in Table 3.

3.1.2.1. Digitization

[63] The analysis have been carried out as for the general case DF inversion. Figure 12 shows the error probability level computed the same way as for the general case DF inversion. The figure shows that $\delta\theta_\pm < 1°$ with a 50% error probability level for $\alpha_Z < 50°$. Concerning the flux and polarization errors, $\delta S < 1$ dB [V^2/Hz] and $\delta V_\pm < 0.10$ at a 1% error probability level for $\beta_{\pm XZ} > 20°$.

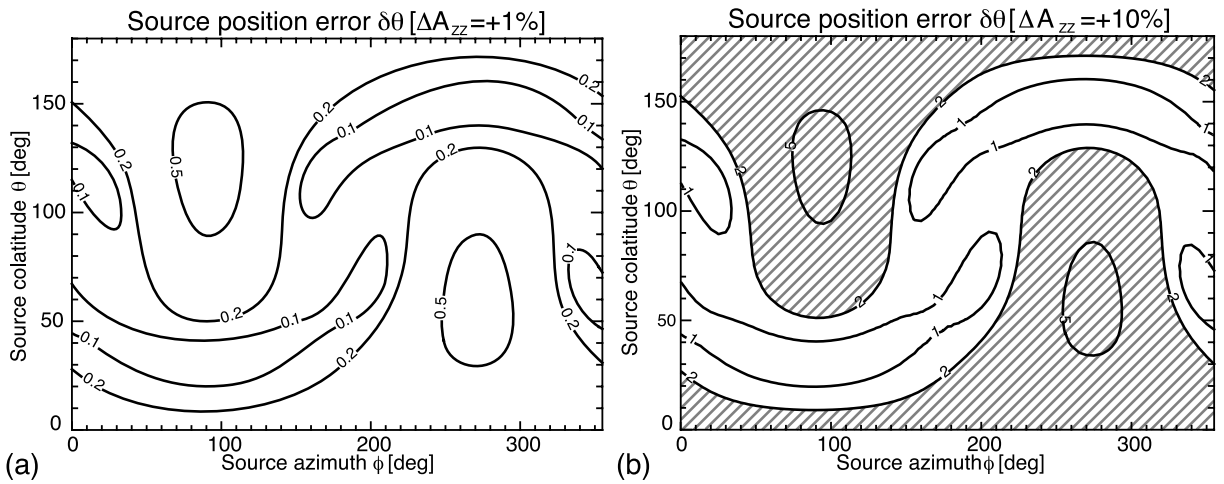

Figure 11. Error on source position $\delta\theta$ in case of (a) 1% and (b) 10% increase of the flux intensity S between the two successive two-antenna data sets in DF mode. Coordinates are in the spacecraft frame. The region for which $\delta\theta > 2°$ has been hatched. The $\delta\theta$ errors are proportional to the flux variation. Lines are isocontours in degree.

Table 2. Direction-Finding Inversion (General Case): Order of Magnitudes for All Types of Errors[a]

Error Type	Level	Data Selection	$\delta\theta$, deg	$\delta S_{\pm}$,[b] dB	$\delta L_{\pm}$[b]	$\delta V_{\pm}$[b]
Digitization	8-bit	$\beta_{\pm XZ} > 20°$	5[b]/1[c]	1.0	0.30[d]	0.10
		$\beta_{\pm XZ} > 40°$	5[b]/1[c]	0.5	0.10	0.05
	12-bit	$\beta_{\pm XZ} > 20°$	0.3[b]	0.5	0.10	$\ll$0.01
SNR	33 dB	$\beta_{\pm XZ} > 20°$	1.2[b]	$\ll$0.1	0.01	$\ll$0.01
	23 dB	$\beta_{\pm XZ} > 20°$	5[b]/2[c]	0.15	0.10	0.02
ΔA_{ZZ}	+10%	$\beta_{\pm XZ} > 20°$	6	1.0	0.12	0.06
	+1%	$\beta_{\pm XZ} > 10°$	0.6	0.1	0.02	0.01
h_Z/h_X	+10%	hatched region of Figure 10a removed	2	0.82	0.11	0.05
		$\alpha_Z < 40°$	4	0.5	0.06	0.03
θ_Z	+2°	hatched region of Figure 10b removed	1	0.22	0.040	0.015

[a]We display the maximum error value for the following parameters: $\delta\theta$ is the angular distance between the input and resulting source position, δS (in dB [V^2/Hz]) the difference between input and resulting flux intensity, δLP and δP the differences between input and resulting linear and total (respectively) degrees of polarization. The results are valid within the following angular selection on the position of the source: $\beta_{\pm XZ} > 20°$ and $S \gg 10^{-16}$ V^2/Hz.

[b]One-percent error probability level.

[c]Fifty-percent error probability level.

[d]With a 50% error probability error, $\delta L_{\pm} \sim 0.10$ in this case.

3.1.2.2. Other Errors

[64] All the other sources of error give the same angular selection criteria and the same errors order of magnitudes on the results. With a selection $\beta_{\pm XZ} > 20°$ and $|\alpha_Z - 90°| > 20°$ (i.e., excluding a 20° region around the plan perpendicular to the Z antenna), we obtain: $\delta S <$ 0.2 dB [V^2/Hz], $\delta\theta < 1°$ and $\delta V_{\pm} < 0.01$.

3.2. Errors Affecting the Antenna Calibration

[65] The same error analysis has been done with the antenna calibration inversion. As the antenna calibration aims at getting the antenna parameters, we focused on the antenna parameters errors even if the inversion provides results for S and V. Moreover, considering that we observed Jupiter emissions with many antenna configuration, that the polarization characteristics of the source are stable and that the unknowns antenna parameters are stable, data selection can be very strict. The error analysis has been performed on all antenna parameters determination but we present only results for the $\vec{h}_Z$ antenna. The results for the two other antennas are very similar. Quantitative results are gathered in Table 4.

3.2.1. Analytical Indeterminations

[66] They occur within two ranges of source directions in the case of angle determination: $\alpha_Z \sim 90°$ (plane perpendicular to the Z antenna) and $\beta_{XZ} \sim 0°$ (plane defined by the (X, Z) pair of antennas). Excluding a 10°-wide region along these two planes leads to a 10^{-5}-degree accuracy on angular results (the computations are done using single precision numbers, i.e., coded on 32 bits. Note that as all other sources of indetermination give accuracies of the order of unity, it is not necessary to make computation using double precision numbers (64 bits coded). Considering the antenna length ratio determination, analytical indeterminations occur mainly in the antenna directions, where $\vec{h}.\vec{E} \sim 0$.

Table 3. DF Inversions Summary: Order of Magnitudes of Errors

DF Inversion	Data Selection	$\delta\theta$	$\delta S_{\pm}$	$\delta L_{\pm}$	$\delta V_{\pm}$
General case	$\beta_{\pm XZ} > 20°$	1°	1.0 dB [V^2/Hz]	0.10	0.10
Circular polarization	$\beta_{\pm XZ} > 20°$ and $\alpha_Z < 50°$	1°	1.0 dB [V^2/Hz]	—	0.10

3.2.2. Digitization

[67] The RPWS digitization has been simulated as above. The 8-bit digitization (corresponding to the Cassini-RPWS receiver) introduces a dispersion in the antenna direction results. The statistical dispersion σ is of

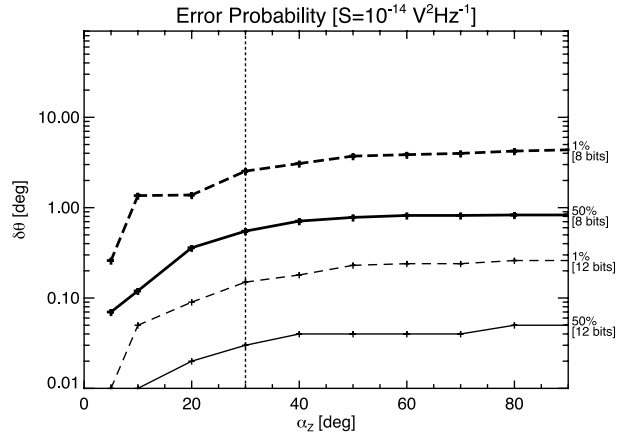

Figure 12. Error probability levels on the source position $\delta\theta$ caused by the digitization for the circular polarization DF inversion. The errors probability levels are displayed for different $\alpha_Z^{\lim}$ and 8-bit/12-bit digitization.

Table 4. Antenna Calibration: Colatitude θ_Z and Azimuth ϕ_Z Results Dispersion for All Kinds of Errors[a]

			θ_Z			ϕ_Z		
Error	Level	Data Selection	δ, deg	σ, deg	Δ, deg	δ, deg	σ, deg	Δ, deg
AGC	8-bit	$\alpha_Z < 45°$, $\beta_{XZ} > 10°$	0.01	0.60	5.71	−0.02	0.96	9.97
	12-bit	$\alpha_Z < 80°$, $\beta_{XZ} > 10°$	0.00	0.10	1.14	0.00	0.16	2.33
SNR	10 dB	$40° < \alpha_Z < 50°$, $\beta_{XZ} > 10°$	1.42	2.41	17.99	−2.86	5.29	43.67
	13 dB	$25° < \alpha_Z < 50°$, $\beta_{XZ} > 10°$	0.16	1.13	13.95	−0.78	1.54	19.84
	20 dB	$15° < \alpha_Z < 70°$, $\beta_{XZ} > 5°$	0.02	0.23	5.82	−0.01	0.32	6.03
	30 dB	$5° < \alpha_Z < 85°$, $\beta_{XZ} > 5°$	0.00	0.00	0.27	0.01	0.04	0.67
h_Z/h_X	+1%	$\alpha_Z < 45°$	−0.17	0.76	5.64	−0.03	1.33	11.00
	+10%	$\alpha_Z < 45°$	−1.11	5.58*c*	32.88	−0.33	10.15	68.11
θ_X	+2°	$\alpha_Z < 45°$	−0.16	0.52	3.35	0.19	1.02	7.54
ϕ_X	+2°	$\alpha_Z < 45°$	0.02	0.59	3.75	0.74	1.43	6.34
U, *Q*	0.01	$\alpha_Z < 45°$	−0.05	0.19	1.04	−0.02	0.35	1.86
	0.05	$\alpha_Z < 45°$	−0.26	0.95	5.41	−0.08	1.78	9.60
	0.10	$\alpha_Z < 45°$	−0.49	1.92	11.44	−0.17	3.61	20.19

[a]The presented results corresponds to the *Z* antenna calibration inversion. The δ, σ and Δ columns correspond, respectively, to the mean relative error, the statistical dispersion and the total width of the distribution (see main text). Similar results can be found for the *X* antenna calibration. Note that errors on the azimuth ϕ_Z are always approximately twice the errors on the colatitude θ_Z: this is a geometrical effect due to the *Z* antenna direction used for our simulation ($\theta_Z = 30°$, $\phi_Z = 90°$).

the order of ∼0.60° with the following angular selection: $\alpha_Z < 45°$ and $\beta_{XZ} > 10°$. Note that the mean value is still zero.

3.2.3. Signal to Noise Ratio

[68] It has been simulated the same way as for the DF inversion error analysis. We have simulated signals with 10, 13, 20 and 30 dB SNR. We define the data selection as follows: The dispersion induced on the final results must be of the order of the digitization one (which is not tunable), with a similar or less restrictive angular selection. These conditions are satisfied when SNR ≥ 20 dB. The angular selection is then $15° < \alpha_Z < 70°$ and $\beta_{XZ} > 5°$.

3.2.4. Preset Parameter Bias

[69] The errors on the fixed parameters have been studied. In the case of the $\vec{h}_Z$ antenna calibration, the parameters h_Z/h_X, θ_X, ϕ_X, θ, φ, *U* and *Q* are assumed to be known. An error on each of these parameters results in a broadening of the θ_Z and ϕ_Z cloud of points when representing them versus α_Z. Qualitative specificity for each case is described below, referring to Figure 13 (quantitative results are given in Table 4).

[70] 1. An error on the antenna length ratio (see Figures 13a and 13b for a 10% higher *Z* antenna) leads to a spindle shape in the (θ_Z, ϕ_Z, α) space. At low α_Z (<30°), the simulated points are distributed over a cone whose projection along the (θ_Z, α_Z) or (ϕ_Z, α_Z) planes gives a "<"-like distribution.

[71] 2. Errors on θ_X or ϕ_X also result in a conic shape at low α_Z (see Figures 13c and 13d). Deviation from the real antenna direction can be as high as 90° if $\alpha_Z \sim 80°$.

[72] 3. Errors on linear polarization (residual component for instance) also result in a broadening of the θ_Z and ϕ_Z cloud of points when representing them versus α_Z. At $\alpha_Z \sim 60°$, we observe deviation from the real antenna direction with a wide ">"-like shape (see Figures 13e and 13f).

[73] 4. Errors on the source position (see Figures 13g and 13h) alter the electrical antenna direction results, even at $\alpha_Z \sim 0°$. An error of 2° on the source colatitude leads to a broadening of the cloud of points, as for the other errors on preset parameters, but at low α_Z we get two branches at ±2° from the input θ_Z value. In the case of a 2° error on the source azimuth, the effect is observed on the resulting ϕ_Z value.

[74] Quantitative results are listed in Table 4. In each case, three numbers are given: (1) $\delta = \langle \theta_Z - \theta_Z^0 \rangle$, the mean relative error of variable θ_Z for $\alpha_Z < \alpha_Z^{\lim}$, with θ_Z^0 an initial guess for the *Z* antenna colatitude; (2) $\sigma = \langle (\theta_Z - \theta_Z^0)^2 \rangle - \langle \theta_Z - \theta_Z^0 \rangle^2$, the statistical dispersion of the θ_Z distribution for $\alpha_Z < \alpha_Z^{\lim}$; (3) $\Delta = \max(\theta_Z) - \min(\theta_Z)$, the total width of the θ_Z distribution for $\alpha_Z < \alpha_Z^{\lim}$.

[75] The same numbers can be defined for ϕ_Z. The upper limit angle $\alpha_Z^{\lim}$ has been fixed at a value of 45° because it is the upper α_Z limit angle in case of the 8-bit digitization of RPWS/HFR (see above).

[76] In summary, the data selection that must be used for antenna direction calibration is the following:

$$15° < \alpha_Z < 45°,\ \beta_{XZ} > 10°,\ \mathrm{SNR} \geq 20\,\mathrm{dB} \qquad (64)$$

where the lower limit on α_Z comes from the 20 dB limit on SNR, and the upper limit on α_Z comes from the digitization process, as does restriction on β_{XZ}. Within this selection, errors on angles are $\lesssim 1°$ if the residual

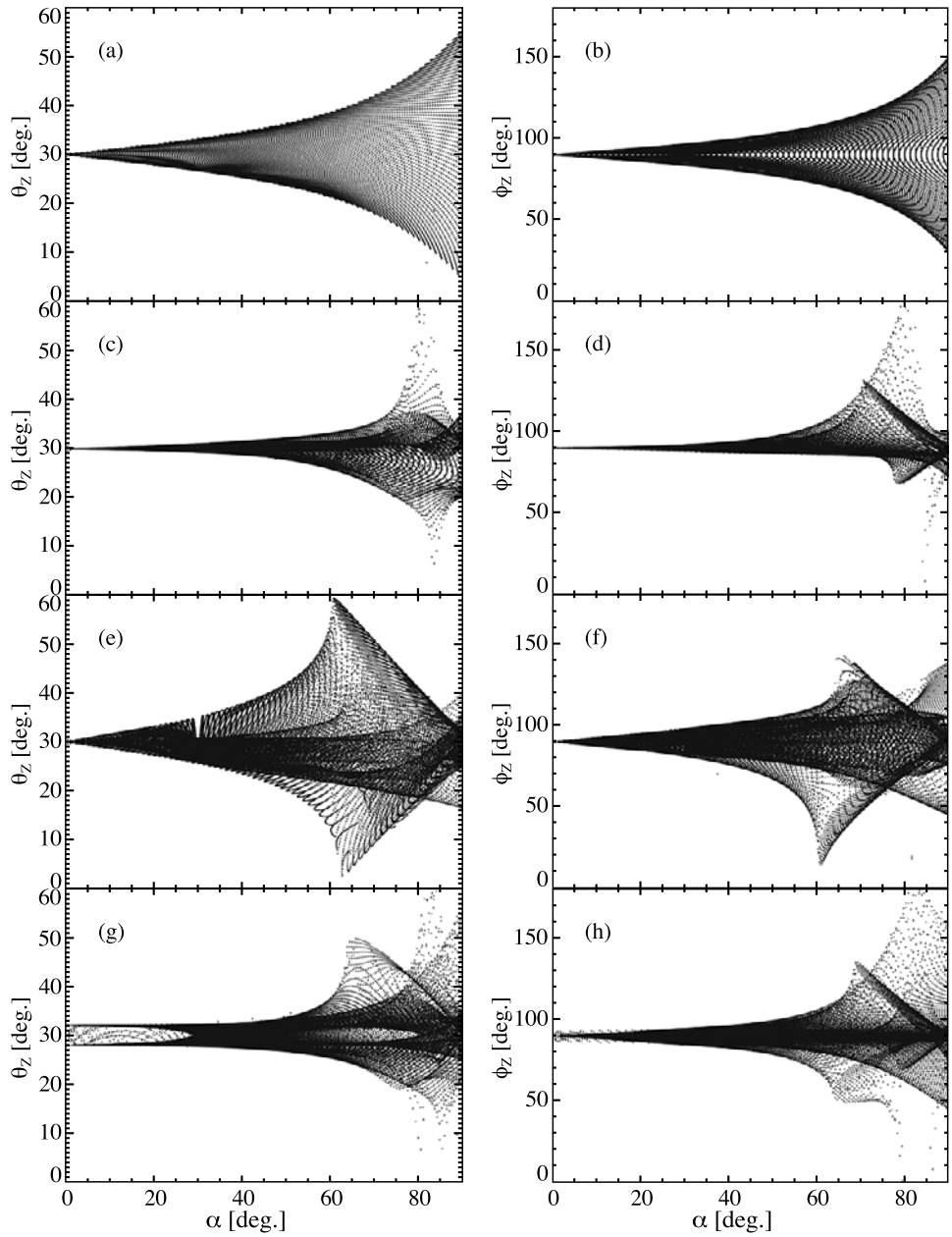

Figure 13. Alteration of θ_Z and ϕ_Z calibration for different biases on preset parameters: (a and b) +10% bias on the Z antenna length h_Z, (c and d) +2° bias on the $+X$ antenna colatitude θ_{+X}, (e and f) 10% residual linear polarization, and (g and h) +2° bias on the source position colatitude θ. Figures 13a, 13c, 13e, and 13g show Z antenna colatitude θ_Z versus α_Z. Figures 13b, 13d, 13f, and 13h show Z antenna azimuth ϕ_Z versus α_Z.

linear polarization level is low (<5%). Note that the angular selection ($\alpha_Z < 45°$) is consistent with the preliminary assumption on source positions set according to the dipole antenna pattern (see section 2.2).

[77] Concerning the antenna length ratio calibration, the data selection that must be used is:

$$\alpha_i > 20°,\ \alpha_j > 20°,\ \mathrm{SNR} \geq 20\,\mathrm{dB} \qquad (65)$$

Table 5. Colatitude and Azimuth of the RPWS Antennas in the Spacecraft Frame, to be Used as Operational Values for the RPWS DF Analysis[a]

	$+X$ Antenna	$-X$ Antenna	Z Antenna
h/h_Z	1.21	1.19	1.0
θ	108.3°	108.0°	29.3°
ϕ	17.0°	163.8°	90.6°

[a]From *Vogl et al.* [2004].

where (i, j) indices correspond to either $(Z, +X)$, $(Z, -X)$ or $(+X, -X)$ pair of antennas. Within this data selection, antenna length ratios have a 0.03 uncertainty.

4. Discussion

[78] The error analysis carried out in the previous section shows that the error amplitude depends mainly on the direction of arrival of the wave with respect to the antenna directions. This leads us to add a data selection criterion to the classical SNR one: some wave directions of arrival have to be excluded to have a good confidence in the results. For the general case DF inversion, the source directions ranges for which we have accurate results are: $\beta_{+XZ} > 20°$ and $\beta_{-XZ} > 20°$; and for the circular polarization case: $\alpha_Z < 50°$ and $\beta_{+XZ} > 20°$, $\beta_{-XZ} > 20°$. Within these regions the order of magnitudes of the errors are the one presented in Table 3.

[79] Concerning the antenna calibration, the angular selection used for the results is given in equations (64) and (65). It is the data selection actually used for antenna calibration discussed by *Vogl et al.* [2004]. The final calibration results are given in Table 5.

[80] The fact that we are using noncalibrated antenna parameters to calibrate others can be seen as a circulus vitiosus. It is actually not, if the calibration steps are done in the following way and because the data sets used for each calibration step have been carefully selected. First, the antenna length ratios have to be calibrated, using noncalibrated antenna directions. The angular selection proposed in equation (65) exclude measurements that strongly depend on the antenna directions, so that roughly calibrated directions are good enough. Then, using these antenna length ratios, one can calibrate the antenna directions in whatever order. Applying several times the calibration process with this ordering on real data shows that the final values and accuracy is obtained at the first step.

[81] Improving the accuracy of the DF analysis results is possible through several means: antenna calibration, orientation of the antennas with respect to the source direction, high SNR (this condition is trivial and will not be discussed here) and finer digitization.

[82] 1. First of all, an accurate antenna calibration is necessary: electrical antenna direction known at $\sim 1°$ and relative effective lengths at $\sim 1\%$. The antenna calibration carried out during the Cassini Jupiter fly-by was done using two inversions techniques (the one presented here and a least square model fitting [see *Vogl et al.*, 2004]). The results were confronted and the final results show an agreement within 1% for antenna effective lengths and 2° for electrical directions. This latter resolution is larger than the expected one which is $\lesssim 1°$. Using the whole set of data recorded during the calibration maneuvers at Jupiter, we computed the Z antenna colatitude θ_Z and represented it versus α_Z (see Figure 14). It is noticeable that the shape of the cloud of points is very similar with the one presented on Figure 13e. One possibility to explain the 2° accuracy on the antenna calibrations results is thus that the emissions used for the antenna calibration may contain some residual linear polarization of the maximum order of 10% (which is actually the accuracy expected for the DF inversion). The assumption that the source position is known can also be tested. As shown on Figure 13g, an indetermination on the source position will influence the antenna calibration results. During the calibration periods programmed at

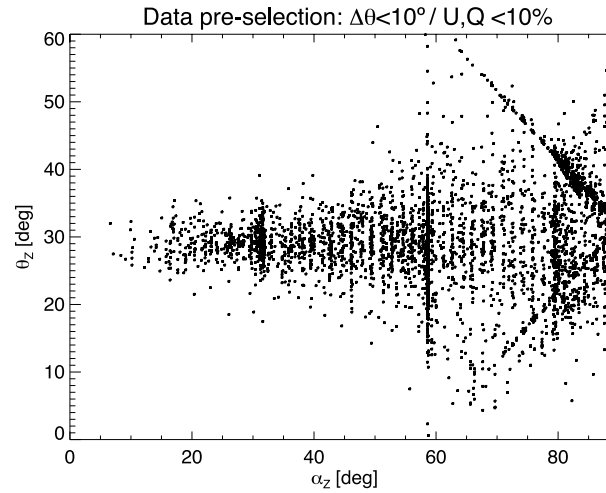

Figure 14. RPWS Calibration data at Jupiter: resulting Z antenna colatitude (θ_Z) versus α_Z. The data preselection applied to the data is the following: the angular distance from the wave direction of arrival to the position of Jupiter is <10°; the degree of linear polarizations U; and Q are <10%. These wave parameters come from a preliminary DF inversion run on the data. The shape of the cloud of points is very similar to the one simulated for a 10% residual linear polarization (see Figure 13e). Thick vertical lines (at $\alpha_Z \sim 30°$ and $\alpha_Z \sim 60°$) corresponds to unwanted emissions still selected by our data preselection (e.g., solar type 3 bursts, that have no polarization and comes from the Sun direction, opposite to the Jupiter direction).

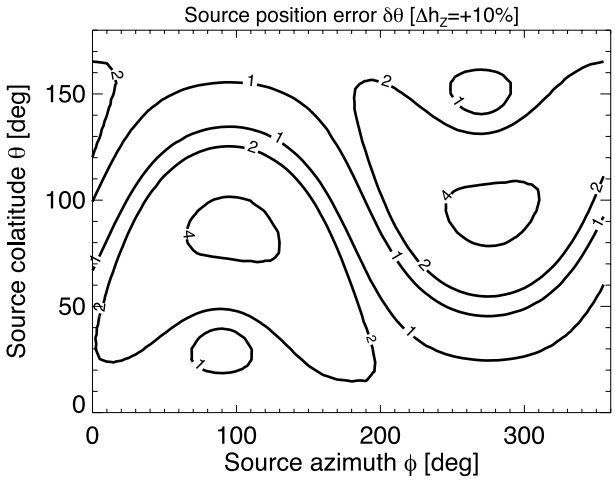

Figure A1. Error on the source position $\delta\theta$ introduced by a +10% bias on the Z antenna length h_Z. Coordinates are in the spacecraft frame. This figure has been computed through an analytical error analysis and has to be compared to Figure 10a, which has been computed through a statistical forward modeling error analysis. Lines are isocontours in degree.

Jupiter, the HOM jovian radio sources that have been selected as calibration sources can be up to 0.6° away from Jupiter's center. The errors induced on the results will thus be of the order of 1°, which will reduce the expected accuracy of the calibration inversion. These effects are at the same order of magnitude as the one induced by the SNR which is ~20 dB in the calibration data and by the receiver digitization.

[83] 2. The source direction of arrival with respect to the electrical antenna directions is critical. The source positions are generally approximately known and it is thus possible to adapt the spacecraft attitude to the observed source, putting the latter into the favorable angular configurations defined in the previous sections, see Table 3 and equations (64) and (65).

[84] 3. Finally, the digitization stage is the most critical one. The RPWS/HFR receiver output data is coded over eight bits. Added together with an AGC device, RPWS/HFR has a 90 dB dynamic range. However we have shown that the 8-bit coding alters the results as would do a ~20 dB equivalent SNR. In the future missions, such as STEREO/WAVES, which radio receiver is an evolution of the receiver built for RPWS/HFR, the receiver will code the output over 12 bits with a similar dynamic range. This will lower the errors introduced by the digitization stage by a factor of 16 ($= 2^{12}/2^8$).

[85] The inversion presented in this paper can be applied to any three-antenna radio receiver that stores instantaneously at least 3 autocorrelation and two cross correlations over its antennas. The STEREO/SWAVES receiver will be able to measure three autocorrelations an three cross correlations, as any pair of monopoles can be used on its two channels. The information will be redundant and thus more robust, but the inversions presented in this paper will be applicable. Having those nine measurements will also permit the use of electromagnetic wave propagation analysis algebraic methods such as described in the work of *Santolík et al.* [2003].

[86] The next step in the development of DF analytical inversions is to take into account extended radio sources. *Manning and Fainberg* [1980] have proposed an inversion technique for extended sources on spinning spacecrafts. In the case of a stabilized spacecraft, the inversion should also be possible as we add only one parameter (the extension σ of the source) to the six wave parameters. We then have seven parameters for seven equations (9 equations in the case of the STEREO/WAVES experiment). If the system of equation is not degenerated it will be possible to solve it either analytically or through a least square model fitting.

[87] The present paper should be considered as a toolkit to exploit at best RPWS DF measurements at Saturn during the Cassini tour (2004–2008), as it allows: (1) to define the data selections that will be applied to obtain the most accurate results and (2) to quantify the corresponding measurements errors (any larger fluctuations can thus be attributed to the radio source itself).

Appendix A: Analytical Error Analysis

[88] The error analysis presented in this paper is based on a statistical forward modeling analysis. This statistical method has been chosen for the simplicity of the treatments and because it was requiring no further algebraic development.

[89] In parallel to the statistical analysis, a fully analytical error propagation analysis has been carried out. This study has required the computation of all the partial derivatives for each parameter given by the inversions. We will not display the whole list of the 95 partial derivatives here. We will nevertheless illustrate this analytical error analysis through one example: the error induced on the source position by a +10% bias on the h_Z antenna length in the general case DF inversion.

[90] Given the following partial derivatives:

$$\frac{\partial \phi}{\partial h_Z} = 0 \tag{A1}$$

$$\frac{\partial \theta}{\partial h_Z} = \frac{\tan^2\theta}{1+\tan^2\theta}\frac{1}{A_{ZZ}\sin\left(2\phi_{+X}\right)}\left[\frac{C^r_{+XZ}\sin\left(\phi+\phi_{+X}\right)}{h_{+X}\sin\theta_{+X}} + \frac{C^r_{-XZ}\sin\left(\phi-\phi_{+X}\right)}{h_{-X}\sin\theta_{-X}}\right] \tag{A2}$$

computed from equations (18) and (19), we can evaluate the source position shift induced by a dh_Z bias on the h_Z antenna length. The azimuth ϕ is not affected as its partial derivative with respect to h_Z is zero. The colatitude θ is altered as:

$$\theta(h_Z + dh_Z) = \theta(h_Z) + \frac{\partial \theta}{\partial h_Z} dh_Z \qquad \text{(A3)}$$

It is then easy to compute the source position shift after having rotated the angular parameters back into the spacecraft frame. The resulting source shift is presented in Figure A1 and has to be compared to Figure 10a. The two figures show exactly the same results, validating thus both approaches.

[91] **Acknowledgments.** We acknowledge support from the Cassini/RPWS team: William S. Kurth, Terry Averkamp, Don Kirchner, and especially principal investigator Don Gurnett from the Department of Physics and Astronomy at the University of Iowa and Alain Lecacheux, Pierre Fédou, and Moustafa Dekkali from LESIA at the Observatory of Meudon. The authors want also to thank Renée Prangé and Milan Maksimovic for many helpful and constructive discussions. They also thank Dieter Vogl, Hans-Peter Ladreiter, and Georg Fischer from the Space Research Institute (IWF) of the Austrian Academy of Sciences. Cassini/RPWS activities at LESIA are supported by the French Centre National d'Études Spatiales (CNES).

References

Dulk, G. A., Y. Leblanc, P. A. Robinson, J.-L. Bougeret, and R. P. Lin (1998), Electron beams and radio waves of solar type III bursts, *J. Geophys. Res.*, *103*, 17,223–17,234.

Fischer, G., and W. Macher (2004), Antenna effective heights and capacitances, paper presented at RPWS Team Meeting, Univ. of Iowa, Iowa City.

Fischer, G., W. Macher, H. O. Rucker, and the Cassini/RPWS Team (2003), Reception properties of the Cassini/RPWS antennas from 1 to 16 MHz, paper presented at EGS-AGU-EUG Joint Assembly, Nice, France.

Gurnett, D. A., et al. (2004), The Cassini radio and Plasma wave science investigation, *Space Sci. Rev.*, *114*, 395–463.

Hamaker, J. P., and J. D. Bregman (1996), Understanding radio polarimetry. III. Interpreting the IAU/IEE definitions of the Stokes parameters, *Astron. Astrophys. Suppl. Ser.*, *117*, 161–165.

Kraus, J. D. (1966), *Radio Astronomy*, McGraw-Hill, New York.

Ladreiter, H. P., P. Zarka, and A. Lecacheux (1994), Direction finding study of Jovian hectometric and broadband kilometric radio emissions: Evidence for their auroral origin, *Planet. Space Sci.*, *42*, 919–931.

Ladreiter, H. P., P. Zarka, A. Lecacheux, W. Macher, H. O. Rucker, R. Manning, D. A. Gurnett, and W. S. Kurth (1995), Analysis of electromagnetic wave direction finding performed by spaceborne antennas using singular-value decomposition techniques, *Radio Sci.*, *30*, 1699–1712.

Lecacheux, A. (1978), Direction finding of a radiosource of unknown polarization with short electric antennas on a spacecraft, *Astron. Astrophys.*, *70*, 701–706.

Lecacheux, A. (2000), Two antenna direction finding with purely circular polarization, paper presented at RPWS Team Meeting, Univ. of Iowa, Iowa City.

Manning, R., and J. Fainberg (1980), A new method of measuring radio source parameters of a partially polarized distributed source from spacecraft observations, *Space Sci. Instrum.*, *5*, 161–181.

Ortega-Molina, A., and G. Daigne (1984), Polarization response of two crossed monopoles on a spacecraft, *Astron. Astrophys.*, *130*, 301–310.

Ortega-Molina, A., and A. Lecacheux (1991), Polarization of Jovian hectometric emission, *J. Geophys. Res.*, *96*, 11,441–11,453.

Rucker, H. O., W. Macher, R. Manning, and H. P. Ladreiter (1996), Cassini model rheometry, *Radio Sci.*, *31*, 1299–1312.

Santolík, O., M. Parrot, and F. Lefeuvre (2003), Singular value decomposition methods for wave propagation analysis, *Radio Sci.*, *38*(1), 1010, doi:10.1029/2000RS002523.

Vogl, D. F., et al. (2004), In-flight calibration of the Cassini-Radio and Plasma Wave Science (RPWS) antenna system for direction-finding and polarization measurements, *J. Geophys. Res.*, *109*, A09S17, doi:10.1029/2003JA010261.

Zarka, P., and B. M. Pedersen (1983), Statistical study of Saturn electrostatic discharges, *J. Geophys. Res.*, *88*, 9007–9018.

Zarka, P., B. Cecconi, and W. S. Kurth (2004), Jupiter's low-frequency radio spectrum from Cassini/Radio and Plasma Wave Science (RPWS) absolute flux density measurements, *J. Geophys. Res.*, *109*, A09S15, doi:10.1029/2003JA010260.

B. Cecconi and P. Zarka, LESIA, Observatoire de Paris, Section de Meudon, 5 Place Jules Janssen, F-92195 Meudon Cedex, France. (baptiste.cecconi@obspm.fr)